Reprints of Published Peer-Reviewed Articles

Excitation functions of heavy residues produced in the $^{14}N + ^{103}Rh$ reaction up to 400 MeV: Analysis of the pre-equilibrium mechanism with the hybrid Monte Carlo simulation model

J. Acharya,[1] S. Mukherjee,[1,*] G. F. Steyn,[2] N. L. Singh,[1] and A. Chatterjee[1]
[1]*Department of Physics, Faculty of Science, M.S. University of Baroda, Vadodara 390002, India*
[2]*iThemba LABS, P.O. Box 722, Somerset West 7129, South Africa*
(Received 24 May 2015; revised manuscript received 27 October 2015; published 12 February 2016)

The excitation functions of heavy residues, produced in the interaction of ^{14}N with ^{103}Rh, have been measured over the projectile energy region from a threshold up to 400 MeV by means of the activation method in conjunction with γ-ray spectroscopy. Cross sections for 15 reaction residues are presented, namely, ^{104}Cd, $^{103-105}Ag$, $^{99-101}Pd$, $^{97,99,101}Rh$, $^{95,97}Ru$, and $^{94-96}Tc$. The experimental data are compared with theoretical model predictions using the hybrid Monte Carlo simulation model as implemented in the recently released ALICE2014 code. The theory assumes that the dominant pre-equilibrium mechanism includes multinucleon and cluster emissions in the initial stages of the interaction between the projectile and the target nucleus. Overall, the theoretical predictions provide a satisfactory agreement with the trend of the present experimental results for most of the observed reaction residues. This provides strong evidence that the underlying reaction mechanisms in the code are appropriately described. Overall, the Obninsk level densities give the best results in the present study.

DOI: 10.1103/PhysRevC.93.024608

I. INTRODUCTION

In heavy-ion reactions, a complex series of processes can occur due to the relatively large number of nucleons involved as well as a large amount of angular momenta that a projectile can transfer to the target nucleus. These processes include the formation of an excited intermediate nucleus in a state far from statistical equilibrium, its equilibration by means of intranuclear interactions, pre-equilibrium emission of nucleons and light clusters, and finally the formation of an intermediate equilibrated nucleus, which further evaporates particles and emits γ rays and/or fission [1–4]. There is a statistical competition between these different reaction mechanisms, which all contribute to the cross sections for the formation of specific heavy residues. It has been known for many years that the small but measurable cross sections for the formation of some of the heavy residues cannot be accounted for by considering only evaporation of particles from an equilibrated compound nucleus. Even at incident energies barely higher than the Coulomb barrier, pre-equilibrium emission of nucleons during the thermalization of the composite nucleus has to be taken into consideration in order to reproduce the formation cross sections of the heavy (targetlike) residues [5].

In recent years, a significant body of experimental data on excitation functions, forward recoil ranges, and angular distributions of residues has been accumulated at incident energies up to 400 MeV [2,3,6–8] in the mass region similar to the present work. This allowed a comprehensive analysis of all the processes which take place, both in the initial projectile-target interaction and during the deexcitation of the nonequilibrated hot nuclei which are produced in the interaction. The analyses of these data have suggested that, in addition to the contributions from projectile fragmentation, deep inelastic collisions, or other nonfusion processes, a significant amount of pre-equilibrium particles is also emitted. The possible importance of pre-equilibrium decay in heavy-ion reactions has been discussed earlier by Blann [9] and Blann and Vonach [10]. Furthermore, a large fraction of α particles which initially participated in the incomplete fusion processes is emitted in the pre-equilibrium stage as well.

The yields of residues formed by α-particle emission should differ appreciably for the respective contributing reaction mechanisms, which depend sensitively on the incident projectile energy. There exists experimental evidence of a pre-equilibrium nucleon and α emission that contribute significantly to the subsequent deexcitation following the fusion of heavy ions [11,12]. In nuclear reactions at intermediate energies, a wide variety of residues is produced. The yields, energy spectra, and angular distributions are valuable information for applications and interdisciplinary fields [13]. The development of phenomenological theories is important in the physics of such reaction data. Earlier, basic reaction models, such as the exciton model [14] and the geometry-dependent hybrid model [11,15], were being employed for analyzing these data, in particular, for their description of pre-equilibrium reactions. However, a comparison of measurements with the model predictions often showed limited success, especially for reactions induced by heavy ions.

Cavinato *et al.* [1] and Buthelezi *et al.* [2,3] presented excitation function data as well as energy spectra and angular distributions of α particles and intermediate mass fragments (IMFs) for $^{12}C + ^{103}Rh$ and $^{16}O + ^{103}Rh$ systems from the Coulomb barrier up to 400 MeV. In order to understand these data, complete fusion and break-up-fusion processes were assumed to depend on the mean-field interaction between the target and the projectile nuclei. The evolution of the system towards equilibrium was studied by following the nucleon-nucleon cascade solving a set of Boltzmann master equations. The model was successful in arriving at a generally good agreement between the measured data and the theoretical predictions.

*Corresponding author: sk.mukherjee-phy@msubaroda.ac.in

Recently, a new version of the code ALICE [11–13,16–18], namely, ALICE2014, has become available, providing a theoretical framework for calculating cross sections for the production of residues at intermediate energies. The new code incorporates the hybrid Monte Carlo simulation (HMS) model for calculating cross sections for pre-equilibrium reactions induced by light and heavy ions. It includes multiple pre-equilibrium emission processes as well as a semiclassical treatment of angular momentum transfer effects. Considering the wide use of the HMS model in applications and to ensure its predictive power, it is important to expose the code to a wide variety of reactions, especially for reactions induced by different medium-mass and heavy ions.

In this paper, excitation functions for the formation of residues in the interaction of ^{14}N projectiles with ^{103}Rh target nuclei were measured from the Coulomb barrier up to 400 MeV. The experiment presented here was designed to establish the extent to which pre-equilibrium emission of α particles is present in heavy-ion reactions leading to the heavy fusionlike and targetlike residues. The use of ^{14}N projectiles enhances the data set for comparisons as data for ^{12}C- and ^{16}O-induced reactions have already been measured on this nucleus [1–3]. It provides a valuable testing ground for the HMS model. In particular, it may be interesting to look for differences in the α-particle and IMF emission spectra as well as the heavy residues left behind from the interactions of a projectile that is not a pure α-like nucleus, such as ^{12}C and ^{16}O. Here we present the excitation functions for heavy reaction residues, and a separate investigation on the emission spectra of light clusters is in progress. Also, the present experimental data, measured with high precision, is a useful addition to the global nuclear database in this mass region.

II. EXPERIMENTAL PROCEDURE

In the present investigation, excitation functions for 15 reaction residues were obtained, namely, ^{104}Cd, $^{103-105}$Ag, $^{99-101}$Pd, ^{97,99,101}Rh, ^{95,97}Ru, and $^{94-96}$Tc for the system of ^{14}N + ^{103}Rh up to 400 MeV using the activation technique in conjunction with off-line γ-ray spectroscopy. The separated sector cyclotron (SSC) of iThemba LABS, capable of accelerating ^{14}N ions up to several tens of MeV nucleon, provided the ^{14}N beam with an incident energy of nominally 400 MeV. The beam formation started with an external cyclotron resonance ion source, followed by injection into a solid pole cyclotron SPC2 which is an injector cyclotron for further acceleration. The SSC provided the final acceleration for the desired beam energy.

The beam current intercepted by the target and beam stop was measured with a Brookhaven Instruments model 1000C current integrator. The accumulated charge was also logged in 10-s intervals by means of the data-acquisition system XSYS. In this way the beam intensity fluctuations during bombardments were monitored. This was performed because beam fluctuations may yield inaccuracies in the results, especially in the case of radionuclides with half-lives shorter than or on the same order of magnitude as the bombardment time if not properly corrected for.

A metallic Rh foil stack was prepared for bombardment with a ^{14}N beam. Self-supporting foils of 99.99% purity were supplied by Goodfellow Ltd. (Cambridge, U.K.). The stack consisted of a single 5-μm-thick Ti monitor foil, followed by several Rh foils with nominal thicknesses of 32.02 mg cm^2. The thickness of the stack was such that it stopped the beam. It was irradiated for 5 h at an incident energy of 395.1 MeV and an average beam current of 50 nA. Afterwards, an autoradiogram of the Ti foil confirmed that the focus of the beam remained on the center of the stack for the entire duration of the bombardment. The beam energy was determined by means of a calibrated 90° analysis magnet with an uncertainty of less than 1 MeV.

The collected γ-ray spectra were analyzed by means of the ENCAMPLUS version 2.01 spectrum analysis software provided by Silena in combination with the spreadsheet program Excel. The ENCAMPLUS software was used for photopeak searches, area, statistical error calculations, background subtraction, and, in a few cases, multiple deconvolution where the photopeaks overlapped. The data sorting program EVAL of the data-acquisition system XSYS was used to extract the current integrator and timer scalar values from the event file logged during the experimental bombardment. The radionuclides produced in the ^{103}Rh target foils were identified by means of their characteristic x and/or γ lines. The decay data used in the analysis were taken from the literature [19].

III. DATA ANALYSIS

A. Experimental cross sections

The experimental production cross sections were obtained from the photopeak area extracted from the measured photon spectra by means of the following expressions:

$$\sigma(\text{mb}) = A_p T_1 K/\tau\varepsilon_\gamma\varepsilon_e I_t N_o \exp[-\lambda(T_m - T)] \times [1 - \exp(-\lambda T_1)](1 \times 10^{-27}),$$

where A_p is the photopeak area of a particular x-ray or γ-ray line, $t = T_1$ is the duration of the bombardment where $t = 0$ is taken as the start time of bombardment, K is a correction factor for beam intensity fluctuations, τ is the live counting time, ε_γ is the branching ratio (intensity) of the photon line, ε_e is the efficiency of the detector, I_t is the total number of beam particles accumulated on the target during bombardment, N_0 is the total number of target nuclei per unit area (cm^{-2}), λ is the decay constant of the particular radionuclide, and T_m is the mean value of the measuring counting interval. All times have units of seconds, and the result of the above equation is given in units of millibarns (mb) (Table I). The factor K is given by

$$K = \frac{\left(\sum_{i=1}^{n} \Delta I_i\right)[\exp(\lambda T_1) - 1]}{\lambda T_1 \sum_{i=1}^{n} \Delta I_i \exp(\lambda h_i)},$$

where n is the number of current integrator readings logged during the bombardment period (scalar values were logged every 10 s), ΔI_i is the beam current integrated (or the number of beam particles on target) during the ith time increment (of 10-s duration) during the bombardment $1 \leqslant i \leqslant n$, and $t = h_i$ is the end of each time increment since the start of the bombardment. Finally, the mean-value time of counting is

TABLE I. Measured cross sections of residues formed in the interaction of ^{14}N with ^{103}Rh up to 400 MeV.

Energy (MeV)	σ (mb)							
	^{103}Ag	^{104}Ag	^{105}Ag	^{104}Cd	^{99}Pd	^{100}Pd	^{101}Pd	
89.4			12.8 ± 1.4			9.32 ± 1.2	8.0 ± 2.3	
110.9			122 ± 13.4	20.3 ± 4.0		24.7 ± 3.2	27.5 ± 5.3	
129.7			228 ± 27.4	32.3 ± 4.3		55.9 ± 8.4	45.8 ± 6.8	
146.7	15.6 ± 3.2	20.7 ± 1.2	223 ± 24.5	30.3 ± 4.1	6.13 ± 0.78	87.6 ± 12.9	71.8 ± 8.5	
162.3	44.8 ± 8.9	103 ± 7.3	331 ± 36.5	45.4 ± 4.5	8.13 ± 1.14	135 ± 18.9	143 ± 11.9	
176.8	55.3 ± 10.5	146 ± 11.8	389 ± 38.6	64.2 ± 6.6	9.06 ± 1.26	166 ± 21.6	190 ± 13.8	
190.5	83.2 ± 15.8	130 ± 9.1	310 ± 34.1	105 ± 13.8	26.5 ± 2.9	234 ± 28.5	204 ± 14.3	
203.5	102 ± 8.6	132 ± 6.2	241 ± 28.9	110 ± 14.3	33.4 ± 4.0	256 ± 31.7	218 ± 14.8	
215.8	96.1 ± 10.8	116 ± 4.6	203 ± 24.6	137 ± 13.8	41.2 ± 4.7	293 ± 35.2	221 ± 14.8	
227.7	94.8 ± 5.7	91.5 ± 3.3	170 ± 19.7	117 ± 14.8	32.3 ± 3.8	287 ± 34.4	230 ± 15.2	
239.0	124 ± 4.3	87.8 ± 3.3	146 ± 12.8	120 ± 15.2	40.5 ± 5.2	326 ± 35.9	228 ± 15.1	
250.0	134 ± 9.8	77.5 ± 3.6	114 ± 10.9	114 ± 15.1	53.4 ± 7.0	171 ± 25.6	184 ± 13.6	
250.9	145 ± 9.6	56.5 ± 2.4	111 ± 10.2	104 ± 13.6	52.8 ± 7.2	131 ± 18.3	202 ± 14.2	
261.7	133 ± 15.9	49.1 ± 2.2	116 ± 10.8	107 ± 14.2	50.5 ± 6.5	190 ± 22.8	195 ± 13.9	
271.9	84.1 ± 5.0	28.2 ± 2.8	126 ± 11.3	114 ± 13.9	44.5 ± 6.0	112 ± 16.8	141 ± 11.9	
281.8	63.0 ± 11.4	20.0 ± 1.0	49.8 ± 5.4	97.8 ± 10.9	45.7 ± 5.5	188 ± 22.6	164 ± 12.8	
291.5	71.9 ± 15.4	19.3 ± 1.6	61.4 ± 5.5	61.7 ± 8.1	38.9 ± 5.5	129 ± 19.4	145 ± 12.0	
300.9	57.3 ± 15.3	17.1 ± 1.7	52.7 ± 5.1	50.9 ± 7.0	45.4 ± 6.7	179 ± 23.3	141 ± 11.9	
310.1	50.7 ± 11.6	16.2 ± 1.6	31.4 ± 3.2	40.8 ± 5.2	36.4 ± 4.9	115 ± 16.1	124 ± 11.1	
319.1	45.0 ± 13.5	12.6 ± 1.5	27.6 ± 3.6	32.4 ± 4.6	38.4 ± 5.4	91.3 ± 13.9	142 ± 11.9	
327.9	39.1 ± 8.3	9.9 ± 1.3	32.1 ± 3.8	30.9 ± 4.4	28.5 ± 4.4	152 ± 25.9	142 ± 11.9	
336.5	38.8 ± 8.2	9.9 ± 0.8	23.6 ± 3.0	35.3 ± 6.2	27.6 ± 3.6	156 ± 26.5	129 ± 11.4	
344.9	31.9 ± 7.0	9.3 ± 1.4	25.2 ± 3.1	26.9 ± 5.8	23.5 ± 3.6	123 ± 20.9	121 ± 11.0	
353.2	34.0 ± 7.1	7.7 ± 1.1	23.1 ± 2.7	28.7 ± 7.0	24.0 ± 3.8	153 ± 30.6	113 ± 10.6	
361.4	25.0 ± 5.7	6.4 ± 0.8	31.2 ± 3.4	29.2 ± 5.9	23.4 ± 3.9	121 ± 19.4	129 ± 11.3	
369.3	28.4 ± 6.1	6.9 ± 1.0	32.2 ± 3.3	22.1 ± 4.9	17.6 ± 3.4	133 ± 23.9	107 ± 10.3	
377.2	20.8 ± 9.6	6.3 ± 0.7	23.9 ± 2.9	22.6 ± 4.5		107 ± 19.2	109 ± 10.4	
384.9	21.1 ± 5.0	6.7 ± 1.5	17.9 ± 2.0	22.5 ± 4.5		118 ± 22.4	94.0 ± 9.7	
392.5	22.1 ± 5.1	7.9 ± 1.3	24.7 ± 2.9	19.3 ± 3.7		150 ± 28.5	95.8 ± 9.8	
400.0	20.7 ± 4.2	6.4 ± 1.2	11.5 ± 2.1	18.8 ± 3.8				

Energy (MeV)	σ (mb)							
	^{97}Rh	^{99}Rh	^{101}Rh	^{95}Ru	^{97}Ru	^{94}Tc	^{95}Tc	^{96}Tc
89.4								
110.9			35.1 ± 4.2					
129.7			80.2 ± 9.6					
146.7		11.0 ± 1.5	113 ± 15.8		20.7 ± 2.7			
162.3		39.5 ± 4.8	149 ± 19.4		18.5 ± 2.4	3.7 ± 0.6	2.7 ± 0.05	
176.8		60.7 ± 9.5	252 ± 35.1		34.2 ± 5.5	5.0 ± 0.8	6.5 ± 0.1	
190.5	9.9 ± 1.2	78.7 ± 11.4	314 ± 33.6	14.5 ± 2.0	63.7 ± 8.9	7.1 ± 1.3	13.2 ± 0.3	13.3 ± 2.4
203.5	20.6 ± 2.3	94.7 ± 12.3	388 ± 46.6	16.4 ± 2.8	82.4 ± 12.3	11.2 ± 2.1	23.9 ± 0.6	19.1 ± 3.1
215.8	19.4 ± 2.5	148 ± 13.7	348 ± 38.3	20.6 ± 3.9	105 ± 13.9	16.8 ± 3.5	34.1 ± 0.8	23.3 ± 5.3
227.7	23.4 ± 3.2	162 ± 15.4	351 ± 45.6	22.0 ± 3.8	147 ± 14.7	17.4 ± 5.4	51.5 ± 1.3	30.2 ± 4.2
239.0	37.5 ± 4.8	171 ± 18.9	375 ± 41.3	41.0 ± 7.0	150 ± 16.5	21.6 ± 7.1	73.9 ± 1.9	35.0 ± 4.1
250.0	36.6 ± 4.7	165 ± 15.3	357 ± 42.8	39.3 ± 6.1	182 ± 20.0	17.7 ± 4.4	96.6 ± 2.5	36.8 ± 2.1
250.9	29.4 ± 3.5	146 ± 19.7	311 ± 33.5	31.2 ± 5.1	131 ± 20.9	16.3 ± 3.3	117 ± 2.7	32.2 ± 6.1
261.7	41.7 ± 5.7	170 ± 23.1	329 ± 46.1	45.9 ± 5.7	154 ± 18.6	22.6 ± 4.1	68.9 ± 1.6	34.3 ± 6.5
271.9	48.6 ± 6.7	254 ± 27.9	314 ± 33.9	56.5 ± 7.0	228 ± 31.9	30.7 ± 7.4	98.5 ± 2.4	40.9 ± 8.6
281.8	37.4 ± 5.5	188 ± 21.7	313 ± 34.4	57.5 ± 7.9	191 ± 28.7	30.4 ± 3.9	111 ± 2.8	37.1 ± 6.3
291.5	58.7 ± 8.7	187 ± 26.2	348 ± 31.3	53.2 ± 7.5	252 ± 45.4	38.7 ± 8.4	100 ± 2.6	43.3 ± 8.2
300.9	52.5 ± 9.3	167 ± 23.4	330 ± 33.0	56.8 ± 7.9	224 ± 42.5	44.6 ± 7.5	134 ± 4.3	39.5 ± 7.1
310.1	60.2 ± 11	171 ± 25.6	303 ± 33.3	61.5 ± 8.0	247 ± 29.6	49.1 ± 6.9	141 ± 4.1	42.4 ± 6.4
319.1	48.9 ± 5.8	149 ± 14.6	281 ± 33.7	65.2 ± 8.4	208 ± 33.3	71.3 ± 11.1	150 ± 4.0	43.2 ± 8.5
327.9	50.2 ± 8.0	150 ± 17.9	263 ± 34.2	63.0 ± 9.5	235 ± 28.2	70.7 ± 9.9	157 ± 5.9	53.6 ± 8.5
336.5	53.1 ± 7.4	175 ± 24.5	283 ± 33.9	68.4 ± 9.6	242 ± 26.6	59.7 ± 4.9	152 ± 5.7	45.5 ± 5.0
344.9	52.0 ± 11	153 ± 19.9	264 ± 42.2	75.9 ± 12.1	255 ± 33.2	79.7 ± 10.9	173 ± 4.2	53.0 ± 4.0

TABLE I. (*Continued.*)

Energy (MeV)	σ (mb)							
	^{97}Rh	^{99}Rh	^{101}Rh	^{95}Ru	^{97}Ru	^{94}Tc	^{95}Tc	^{96}Tc
353.2	53.7 ± 11	150 ± 24.2	267 ± 37.4	78.5 ± 10.2	236 ± 40.1	68.3 ± 8.8	182 ± 5.7	59.0 ± 3.6
361.4	45.7 ± 5.5	165 ± 23.1	233 ± 34.9	76.1 ± 16.0	241 ± 43.4	70.5 ± 6.8	183 ± 5.8	46.5 ± 1.6
369.3	46.6 ± 12	129 ± 21.9	244 ± 39.0	81.7 ± 13.8	229 ± 43.5	91.7 ± 10.8	168 ± 3.4	55.2 ± 2.7
377.2	41.6 ± 3.8	130 ± 22.8	201 ± 33.6	79.9 ± 15.2	210 ± 37.8	86.3 ± 6.1	187 ± 6.4	49.2 ± 9.2
384.9	44.6 ± 15	139 ± 24.7	216 ± 32.1	78.1 ± 17.9	188 ± 37.6	79.1 ± 10.5	160 ± 5.1	58.4 ± 2.5
392.5	40.1 ± 8.3	142 ± 26.9	209 ± 29.3	83.4 ± 18.3	205 ± 45.1	59.8 ± 8.0	165 ± 5.1	61.4 ± 2.4
400.0	41.6 ± 5.4	107 ± 17.1	124 ± 14.9	75.8 ± 15.9	169 ± 32.1	56.7 ± 8.5	162 ± 4.8	56.2 ± 1.8

given by

$$T_m = -\frac{1}{\lambda}\ln\left[\frac{\exp[-\lambda(T_3 - T_2)]}{-\lambda(T_3 - T_2)}\right],$$

where $t = T_2$ denotes the start time of the counting period and $t = T_3$ denotes the end time of the counting period, relative to $t = 0$ being the start time of the bombardment.

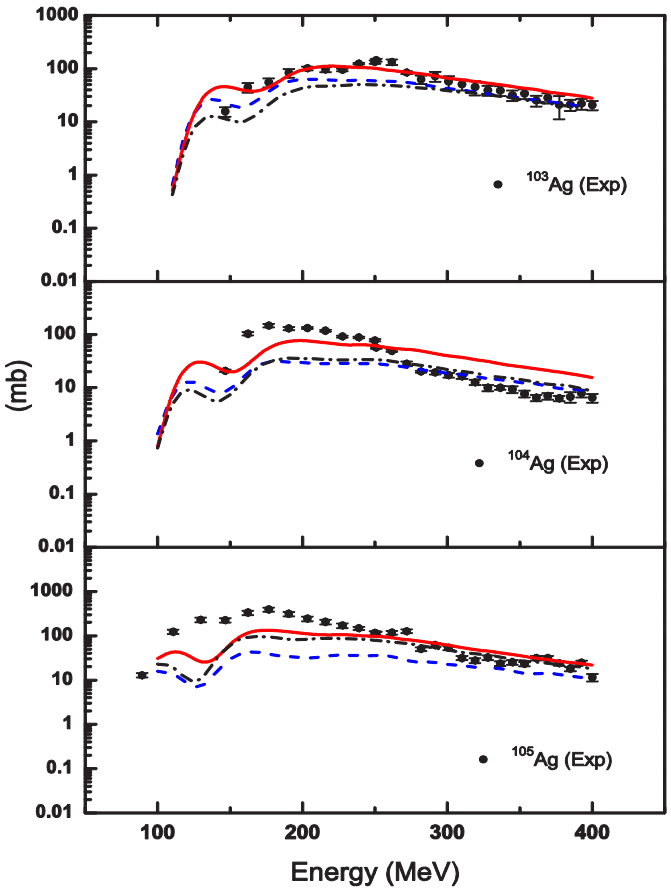

FIG. 1. Excitation functions of Ag residues formed in the interaction of ^{14}N with ^{103}Rh as indicated. The solid symbols are the experimental results of this paper. The calculated excitation functions are shown as the red solid curves (OB level density), the blue dashed curves (FG level density), and the black dashed-dotted curves (KR level density) as obtained with the nuclear reaction code ALICE2014.

The factor K may become important whenever the half-life of a particular radionuclide is shorter than or on the same order of magnitude as the bombardment time. In such cases, K can be strongly dependent on fluctuations in the beam intensity and become different from a normative value of unity.

B. Detector calibration

Both energy and efficiency calibrations were performed using standard sources of ^{133}Ba and ^{152}Eu, traceable to the Bureau International des Poids et Mesures. The ^{133}Ba source has a number of strong characteristic x-ray lines at 30.6 keV (34.4%), 31.0 keV (63.5%), and 35.0 keV (18.8%), which were useful for the calibration of the APTEC planar high-purity (HP)Ge x-ray detector. The ^{152}Eu has strong γ lines over the entire energy region from 121 to 1408 keV. Although the energy response of both the APTEC x-ray and EG&G ORTEC coaxial HPGe γ-ray detectors were very nearly linear, third-order polynomial fits were used for the energy calibration.

C. Uncertainty analysis

The uncertainty values of the experimental cross sections were estimated by summing all the contributing uncertainties in quadrature and were typically between 15% and 20%.

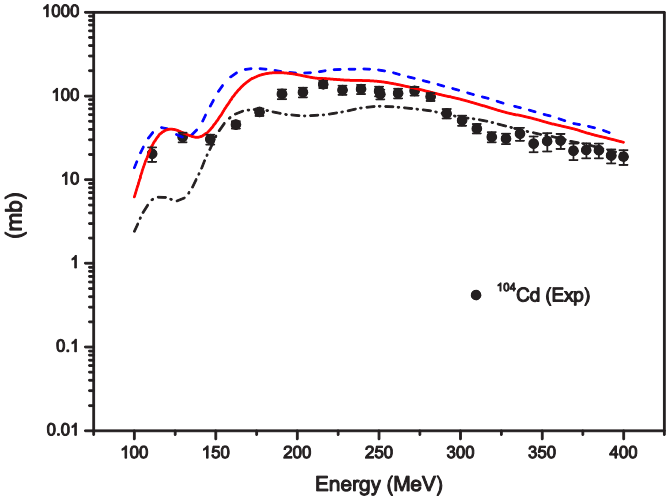

FIG. 2. Excitation function of ^{104}Cd residues formed in the interaction of ^{14}N with ^{103}Rh. Also see the caption for Fig. 1 for more details.

This includes the counting statistics, beam loss as a result of nonelastic nuclear interactions (2%), target thickness (10%), accumulated beam charge (2%), detector efficiency (5%), counting geometry (5%), photopeak integration (2%), and branching ratios (2%).

IV. THEORETICAL CALCULATIONS

Theoretical calculations were performed using the recently released computer code ALICE2014 [11–13,16–18]. This nuclear reaction code is the latest version of the so-called HMS-ALICE codes in which pre-equilibrium emission of both nucleons and light clusters is based on the HMS model [17]. All cascades are terminated in the Weisskopf-Ewing evaporation model [20], and the equilibrium emission of both nucleons and light clusters can be selected. The options for emission were taken to be similar, i.e., both pre-equilibrium as well as equilibrium emission of n, p, ^{2}H, ^{3}H, ^{3}He, and ^{4}He were chosen for the present calculations. Calculations were performed with three forms of the nuclear level density: Kataria-Ramamurthy (KR) and Kapoor [21], Obninsk [22] (OB), and backshifted Fermi gas (FG). The OB and KR forms do not have any adjustable parameters. For FG we performed the calculations with "a" $= A/9$, which is the default value. The changes resulting in varying a in the range of $A/7 - A/11\,\mathrm{MeV}^{-1}$ is 10% or less throughout the energy region, and this is shown in Fig. 7. The ALICE2014 code contains an error in the calculation of the KR level densities which we have corrected. The other input parameters were set to the default values of the code. Further details of the code are available in the literature [11–16].

V. RESULTS AND DISCUSSION

The experimental cross sections are presented in Table I and are compared with the ALICE2014 theoretical predictions in Figs. 1–6. The calculated excitation functions are shown as dashed curves (using Obninsk level densities), solid curves (using Fermi gas level densities), and dashed-dotted curves (using Kataria-Ramamurthy level densities). In the case of cumulative cross sections for the formation of the observed residues, the fractional contributions from precursor decay were summed to the directly produced contribution. These fractional precursor contributions were obtained by adopting the procedure given in the literature [1,2].

The silver residues observed in this paper are $^{103-105}$Ag, shown in Fig. 1. The experimental excitation function of ^{103}Ag exhibits a broad peak with a maximum of $\sim$145 mb at 250.9 MeV, beyond which the slope of the curve decreases

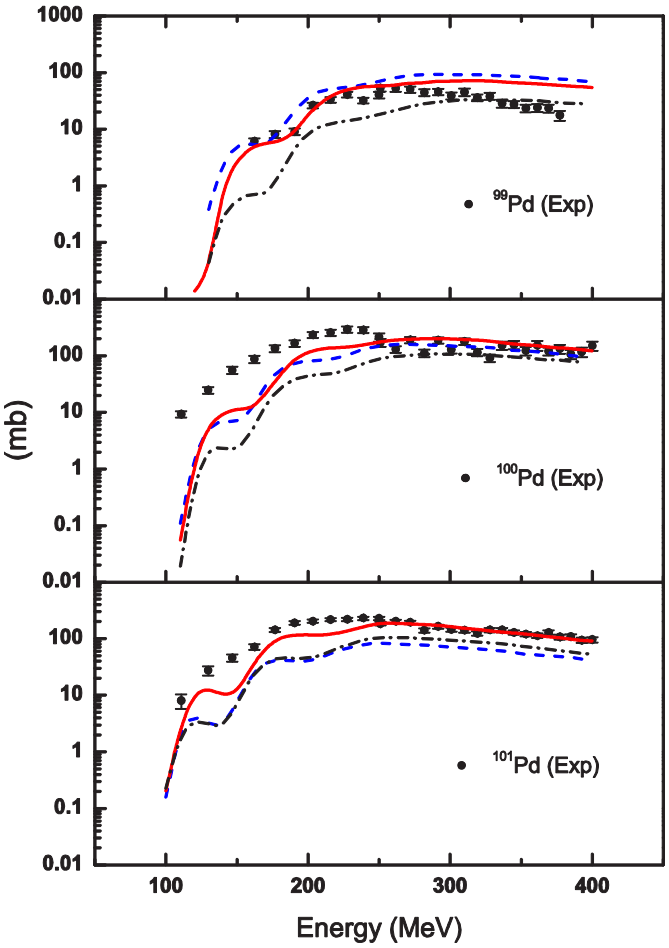

FIG. 3. Excitation functions of Pd residues formed in the interaction of ^{14}N with ^{103}Rh as indicated. Also see the caption for Fig. 1 for more details.

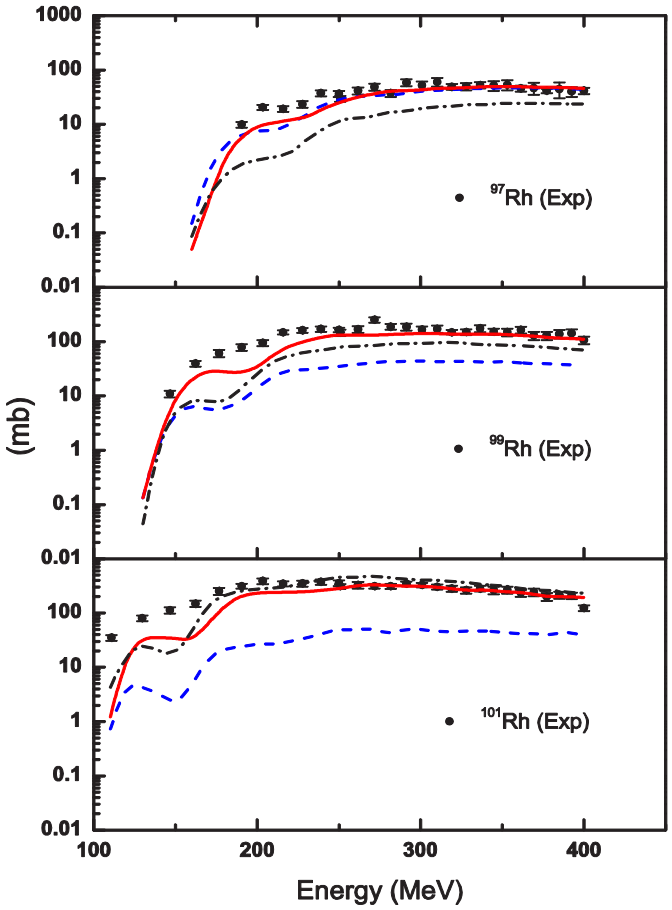

FIG. 4. Excitation functions of Rh residues formed in the interaction of ^{14}N with ^{103}Rh as indicated. Also see the caption for Fig. 1 for more details.

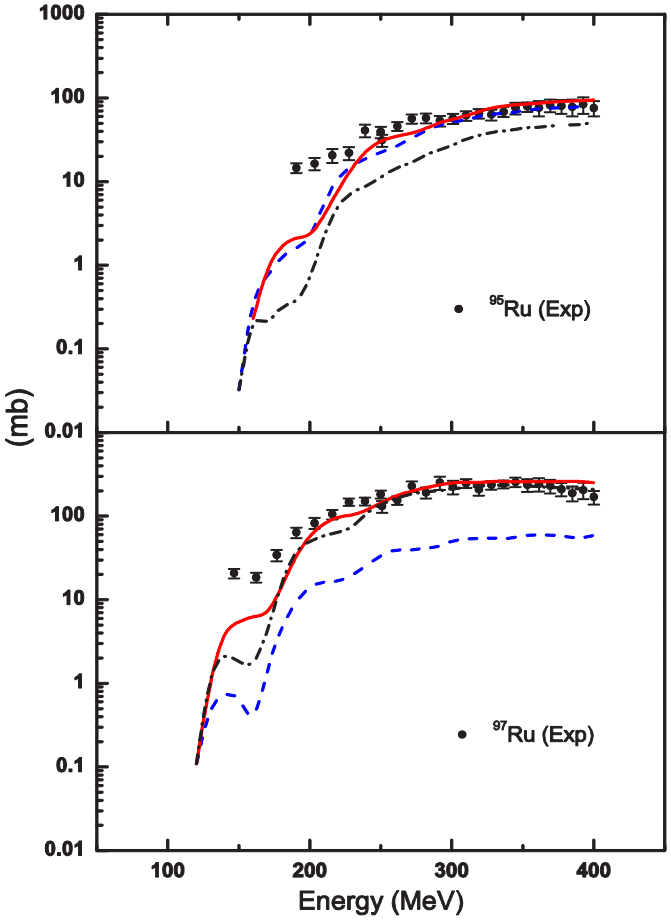

FIG. 5. Excitation functions of Ru residues formed in the interaction of ^{14}N with ^{103}Rh as indicated. Also see the caption for Fig. 1 for more details.

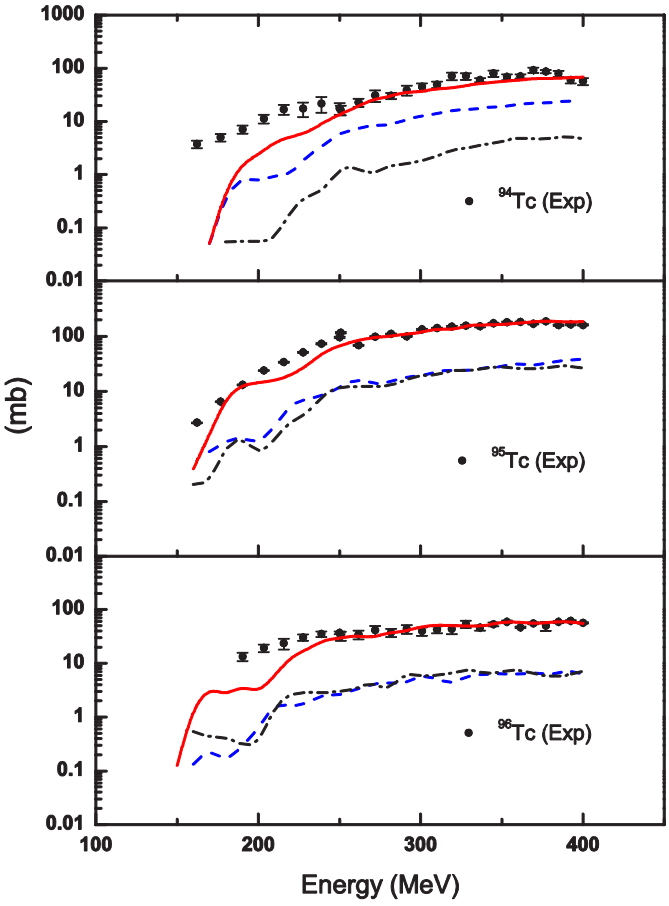

FIG. 6. Excitation functions of Tc residues formed in the interaction of ^{14}N with ^{103}Rh as indicated. Also see the caption for Fig. 1 for more details.

monotonically towards higher energies. The excitation functions of ^{104}Ag and ^{105}Ag show similar trends, reaching maxima of ∼146 and ∼389 mb at 176.8 MeV, respectively. The theoretical predictions with all three level-density formalisms (OB, FG, and KR) are reasonable in the case of the ^{103}Ag isotope. In the case of ^{104,105}Ag, both FG and KR give a better agreement than the OB level density, above 250 MeV. A more pronounced underprediction is consistently observed with all three level densities below 250 MeV. However, the discrepancy is more pronounced in the case of FG and KR as compared to the OB level density for ^{104,105}Ag isotopes.

The only residue of cadmium observed in this paper is ^{104}Cd, shown in Fig. 2. Here the calculations with all three level-density formalisms show nearly identical results, which are quite close to the data. The excitation function is rather structureless and almost constant between 200 and 300 MeV. The measurements seem to support the three local maxima predicted by the calculations but shifted towards higher energies. The experimental maximum is 137 mb at 215.8 MeV. Both the FG and the OB level densities give similar results in the entire energy region, whereas the KR level density underestimates the experimental results below 150 MeV.

The observed palladium residues are $^{99-101}$Pd, shown in Fig. 3. The shapes of these excitation functions are also quite structureless, rising rather gently from their respective thresholds to exhibit very broad peaks. Beyond the peak maxima, the decreasing trend of the excitation functions is quite small, thus their appearance seems almost flat towards higher energies. The calculations show a marked underprediction towards lower energies in the cases of ^{100}Pd and ^{101}Pd. This discrepancy is not observed in the case of ^{99}Pd, however, an overprediction is evident towards higher energies for both OB and FG level densities. The overall agreement with the measurements is markedly better when using the OB level density in comparison with those given by FG and KR.

The excitation functions for the ^{97,99,101}Rh, ^{95,97}Ru, and $^{94-96}$Tc residues exhibit very similar trends as shown in Figs. 4–6. No prominent peaks or local maxima are observed. Rather, the excitation functions rise from their respective thresholds up to nearly constant plateaus towards higher energies. The theoretical calculations reproduce the plateaus very satisfactorily when the OB level densities are used. In contrast, rather serious underpredictions are evident in some of the cases, that is, Rh, Ru, and Tc isotopes where FG and KR level-density options are used. Overall in the above-mentioned three sets of isotopes, OB gives by far the best agreement in comparison with the FG and KR options of level density.

Figures 8–10 show the comparison of three of the presently measured excitation functions (^{14}N + ^{103}Rh) with those mea-

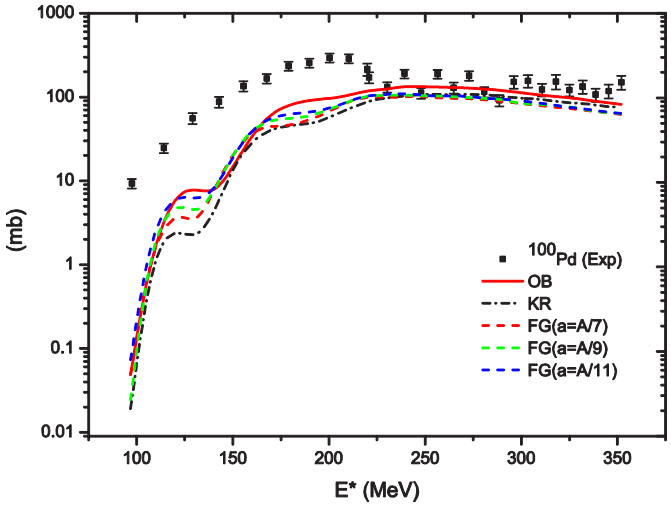

FIG. 7. Excitation function ^{100}Pd residue in the $^{14}N + ^{103}Rh$ reaction with different level-density options.

sured earlier for the systems of ^{12}C and $^{16}O + ^{103}Rh$ up to 400 MeV [1–3]. Same global parameters were used in the HMS model calculations in all three systems. Three typical excitation functions for the residues, ^{94}Tc, ^{99}Rh, and ^{100}Pd

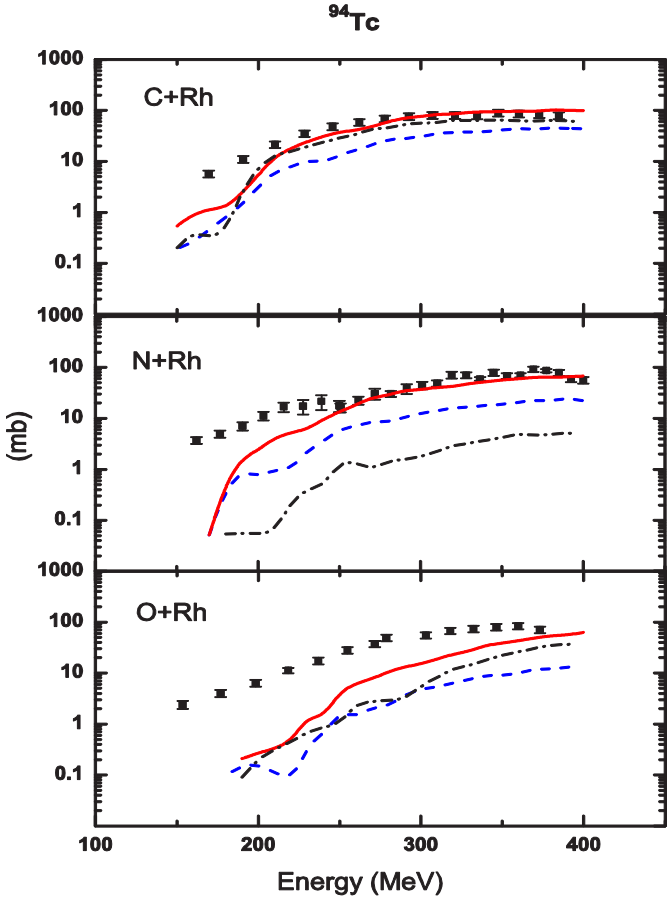

FIG. 8. Intercomparison of excitation functions of ^{94}Tc for ^{12}C, ^{14}N, and $^{16}O + ^{103}Rh$ systems. Theoretical calculations with the HMS model are shown by the solid red curves (OB), the dashed blue curves (FG), and the black dashed-dotted curves (KR).

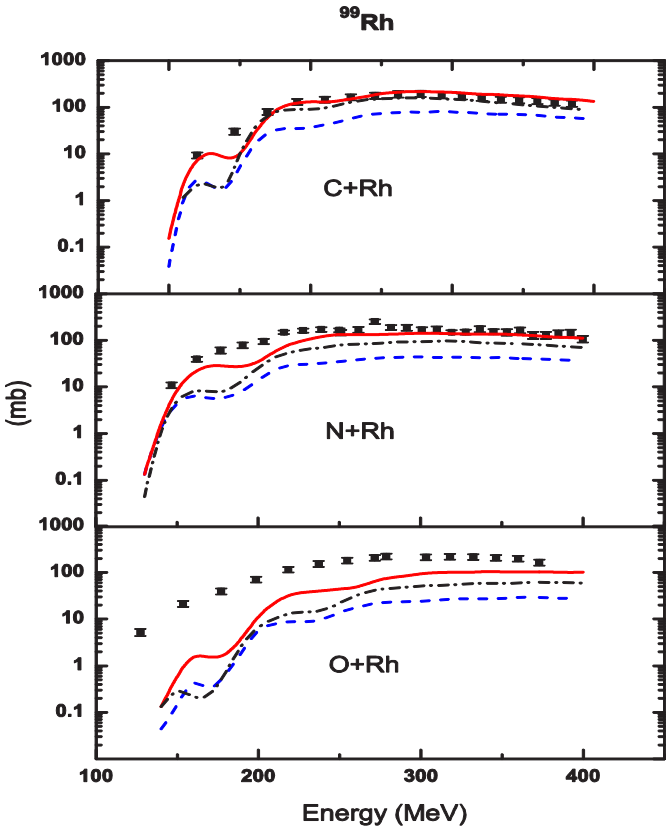

FIG. 9. Intercomparison of excitation functions of ^{99}Rh for ^{12}C, ^{14}N, and $^{16}O + ^{103}Rh$ systems. Theoretical calculations with the HMS model are shown by the solid red curves (OB), the dashed blue curves (FG), and the black dashed-dotted curves (KR).

were selected for intercomparison of the systems with the present HMS model calculations. In Fig. 8, it may be observed that the excitation function for ^{94}Tc gives the best results for the OB level density for the $^{12}C + ^{103}Rh$ system between 200 and 400 MeV, whereas for $^{14}N + ^{103}Rh$ the results are better with the OB level densities between 250 and 400 MeV. In the case of $^{16}O + ^{103}Rh$, there is a gross underestimation by all three level densities. In the case of the excitation function of ^{99}Rh (Fig. 9), both ^{12}C and $^{14}N + ^{103}Rh$ systems give similar and best results with the OB level density, whereas for the $^{16}O + ^{103}Rh$ system the calculations underestimate the experimental results. In Fig. 10, $^{12}C + ^{103}Rh$ gives the best agreement with all three level densities (OB, KR, and FG) as compared to the ^{14}N and $^{16}O + ^{103}Rh$ systems. In general, it may be concluded that the present theoretical and experimental results are quite close in agreement with the $^{12}C + ^{103}Rh$ system, whereas for the $^{16}O + ^{103}Rh$ system the theoretical results significantly underestimate the experimental results.

A. Level-Density Analysis

The absolute values of level density are vastly different. This is illustrated in Fig. 11 for one case. It will be noticed that at 200-MeV excitation, the OB level density is 20 orders of magnitude less than the FG level density with $a = A/7\,\mathrm{MeV}^{-1}$, however, it is the excitation energy

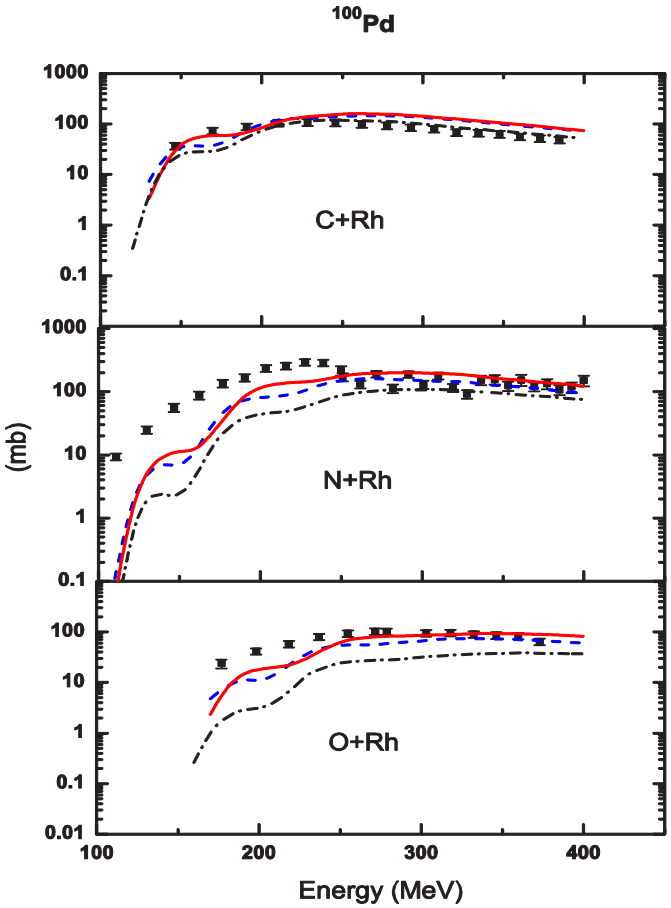

FIG. 10. Intercomparison of excitation functions of ^{100}Pd for ^{12}C, ^{14}N, and ^{16}O + ^{103}Rh systems. Theoretical calculations with the HMS model are shown by the solid red curves (OB), the dashed blue curves (FG), and the black dashed-dotted curves (KR).

dependence that matters and not the absolute value of the level density. As seen in the figure, the OB level density has a distinctly different energy dependence as compared to the other level-density forms. It is important to note that in the original formulation of the KR level density [21] excitation energies above 60 MeV were not considered. For higher excitation the FG ($a = A/9\,\mathrm{MeV}^{-1}$) level-density form scaled to the 60-MeV KR value is used in ALICE2014. The OB level density was formulated relatively recently as compared to FG and KR, and it is heartening to note that overall it performs better in comparison with the present data. It is true that specific cases show differing degrees of agreement in different energy ranges, however, this is only to be expected for calculations of a global nature without adjustable parameters.

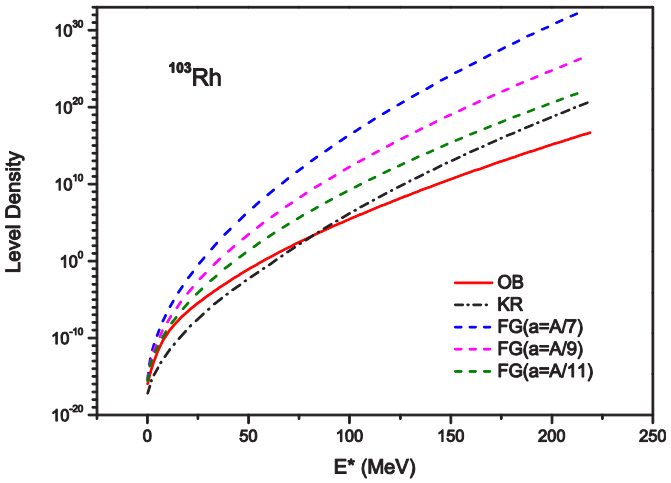

FIG. 11. Level density of the ^{103}Rh isotope as a function of excitation energy for $l = 0$ for different options as indicated.

As already mentioned earlier, varying the value of the FG level-density parameter between $A/7$ and $A/11\,\mathrm{MeV}^{-1}$ only results in small changes. As an example of this insensitivity, Fig. 7 shows calculations using $a = A/7$, $A/9$, and $A/11$ for the excitation function of the ^{100}Pd residue. Consequently, a value of $A/9$ was adopted throughout for the remainder of the calculations.

VI. SUMMARY AND CONCLUSIONS

Excitation functions for 15 reaction residues were measured in the ^{14}N + ^{103}Rh system up to 400 MeV. The present theoretical analysis was performed by using the HMS model using three different forms of the nuclear level density, namely, OB, KR, and backshifted FG. We have corrected an error in ALICE2014 which was leading to incorrect results for KR level densities. In the HMS model the decay of the composite system is initially followed in terms of nucleon-nucleon collisions. Unlike previous versions, there are no adjustable parameters in ALICE2014 for this phase of the reaction. After the system cools sufficiently, the usual statistical model is applied, and in this phase the nuclear level density plays a crucial role in deciding the final population of the residues. At each step of the statistical decay, particle emission rates depend on the ratio of level densities of the residual and parent systems.

The overall trends of the predicted excitation functions are satisfactory. The absolute values generally agree well with the experimental data for lighter isotopes and at energies above 200 MeV with the OB level density. The latter region is the one where pre-equilibrium emission of nucleons and light clusters dominates and is therefore a more important region for the test of the present pre-equilibrium model. Considering the various options for the level densities, it was observed that the Kataria-Ramamurthy level densities lead to predictions very far from the data. In general it may be concluded that the calculations with the HMS model (ALICE2014) with the OB level densities has qualitative trends similar to the data and reasonable quantitative agreement at the higher energies. The OB level density gives a fairly good description of the excitation functions for the observed isotopes of Cd, Ag, Pd, Rh, Ru, and Tc in that the general features are reproduced. The new code ALICE2014, which incorporates pre-equilibrium multinucleon and cluster emissions in addition to the emission of single nucleons, satisfactorily describes the underlying mechanism for the production of heavy residues induced by medium-mass ions at intermediate energies. In general, it may also be concluded that the present experimental and theoretical calculations are in close agreement with those obtained earlier for the ^{12}C + ^{103}Rh system.

ACKNOWLEDGMENTS

One of the authors (G.F.S.) thanks RSICC, ORNL, USA for providing the ALICE2014 code for the present theoretical analysis. S.M. thanks the Chinese Academy of Sciences for the support in the form of President's International Fellowship Initiative (PIFI) Grant No. 2015-FX-04 to visit IMP-CAS, Lanzhou, China.

[1] M. Cavinato, E. Fabrici, E. Gadioli, E. Gadioli Erba, P. Vergani, M. Crippa, G. Colombo, I. Redaelli, and M. Ripamonti, Phys. Rev. C **52**, 2577 (1995).
[2] E. Z. Buthelezi, F. Cerutti, E. Gadioli, G. F. Steyn, S. H. Connell, and A. A. Cowley, Nucl. Phys. A **753**, 29 (2005).
[3] E. Z. Buthelezi, F. Cerutti, E. Gadioli, G. F. Steyn, A. Pepe, S. H. Connell, and A. A. Cowley, Eur. Phys. J. A **28**, 193 (2006).
[4] M. B. Chadwick, P. G. Young, S. Chiba, S. C. Frankle, G. M. Hale, H. G. Hughes, A. J. Koning, R. C. Little, R. E. MacFarlane, R. E. Prael, and L. S. Waters, Nucl. Sci. Eng. **131**, 293 (1999).
[5] P. Vergani, E. Gadioli, E. Vaciago, E. Fabrici, E. Gadioli Erba, M. Galmarini, G. Ciavola, and C. Marchetta, Phys. Rev. C **48**, 1815 (1993).
[6] E. Gadioli, C. Birattari, M. Cavinato, E. Fabrici, E. Gadioli Erba, V. Allori, F. Cerutti, A. Di Filippo, S. Vailati, T. G. Stevens, S. H. Connell, J. P. F. Sellschop, F. M. Nortier, G. F. Steyn, and C. Marchetta, Nucl. Phys. A **641**, 271 (1998).
[7] E. Gadioli, M. Cavinato, E. Fabrici, E. Gadioli Erba, C. Birattari, I. Mica, S. Solia, G. F. Steyn, S. V. Förtsch, J. J. Lawrie, F. M. Nortier, T. G. Stevens, S. H. Connell, J. P. F. Sellschop, and A. A. Cowley, Nucl. Phys. A **654**, 523 (1999).
[8] C. Birattari, M. Bonardi, M. Cavinato, E. Fabrici, E. Gadioli, E. Gadioli Erba, F. Groppi, M. Bello, C. Bovati, A. Di Filippo, T. G. Stevens, S. H. Connell, J. P. F. Sellschop, S. J. Mills, F. M. Nortier, G. F. Steyn, and C. Marchetta, Phys. Rev. C **54**, 3051 (1996).
[9] M. Blann, Nucl. Phys. A **235**, 211 (1974).
[10] M. Blann and H. K. Vonach, Phys. Rev. C **28**, 1475 (1983).
[11] M. Blann, Annu. Rev. Nucl. Sci. **25**, 123 (1975).
[12] M. Blann and M. B. Chadwick, Phys. Rev. C **57**, 233 (1998).
[13] M. B. Chadwick and P. Obložinský, Phys. Rev. C **50**, 2490 (1994).
[14] E. Gadioli, E. Gadioli Erba, and P. G. Sona, Nucl. Phys. A **217**, 589 (1973); E. Gadioli and E. Gadioli Erba, Nucl. Instrum. Methods **146**, 265 (1977).
[15] M. Blann, Phys. Rev. Lett. **28**, 757 (1972).
[16] M. Blann and A. Y. Konobeev, Precompound Cluster Decay in HMSALICE (2008) (unpublished), available in documentation supplied with RSICC code package PSR-550, https://rsicc.ornl.gov/
[17] M. Blann, Phys. Rev. C **54**, 1341 (1996).
[18] S. G. Mashnik, K. K. Gudima, A. J. Sierk, M. I. Baznat, and N. V. Mokhov, CEM03.01 User Manual, LANL Report No. LA-UR-05-7321, 2005 (unpublished).
[19] *Table of Isotopes*, 8th ed., edited by R. B. Firestone and V. S. Shirley (Wiley, New York, 1996); R. B. Firestone and L. P. Eckström, *WWW Table of Radioactive Isotopes*, Version 2.1 (2014), available from http://ie.lbl.gov/toi
[20] V. F. Weisskopf and D. H. Ewing, Phys. Rev. **57**, 472 (1940).
[21] S. K. Kataria, V. S. Ramamurthy, and S. S. Kapoor, Phys. Rev. C **18**, 549 (1978).
[22] A.V. Ignatyuk, J. L. Weil, S. Raman, and S. Kahane, Phys. Rev. C **47**, 1504 (1993).

Neutron emission in ^{19}F-induced reactions

Jaimin Acharya, S. Mukherjee,* A. Chatterjee, and N. L. Singh
Department of Physics, The M.S. University of Baroda, Vadodara 390002, India

K. Ramachandran, P. C. Rout, K. Mahata, Vishal Desai, E. T. Mirgule, S. V. Suryanarayana, B. K. Nayak, and A. Saxena
Nuclear Physics Division, Bhabha Atomic Research Centre, Mumbai 400085, India

G. F. Steyn
iThemba LABS, Somerset West, South Africa

(Received 15 August 2017; revised manuscript received 30 November 2017; published 14 March 2018)

We measured neutron emission spectra for ^{19}F-induced reactions on ^{181}Ta, ^{89}Y, and ^{51}V at beam energies of 130, 140, 145, and 150 MeV. Measurements were made using liquid scintillator detectors at eight angles in the range of $25^\circ - 143^\circ$ using time-of-flight and pulse-shape discrimination. A comparison has been made with ALICE2014 and PACE4 calculations to understand the role of incomplete fusion and pre-equilibrium effects. Global predictions with ALICE2014 without parameter adjustment gives a fair agreement with the measured data.

DOI: 10.1103/PhysRevC.97.034607

I. INTRODUCTION

Many attempts have been made to understand the pre-equilibrium process in terms of nucleon-nucleon interactions within the target nucleus [1–6]. In the past few decades, several quantum mechanical theories have been proposed that can provide a way of calculating cross sections of pre-equilibrium processes without the uncertainties of semi-classical approximations. With increasing bombarding energy, especially at forward angles and higher emission energies, pre-equilibrium effects can be pronounced and in some cases it could be the dominant reaction mechanism.

From a nuclear data standpoint, it is not sufficient to have a theory that will fit the available experimental data with parameter values adjusted from case to case. Rather a theory with a global perspective that can be used with some confidence to predict cross sections of reactions that have not yet been measured or are difficult or not possible to measure is needed. Several computer codes are available for quantum mechanical theories so it is desirable to test their ability to calculate the required cross sections. More importantly, we want to know how accurately they are able to calculate without arbitrary variation of parameters.

During the past few decades the Monte Carlo pre-equilibrium model has been developed, which provides certain advantages for use in modeling nuclear reactions and generating Evaluated Nuclear Data File (ENDF) databases. The initial formulation by Blann [7] was subsequently expanded to include the treatment of ejectile angular and energy distribution in a new pre-compound model [8]. Another pre-compound Monte Carlo model was introduced to take care of the treatment of cluster-induced reactions [9]. This approach is valuable because of its ability to accurately model a comprehensive variety of nuclear reaction mechanisms that occur for projectiles with incident energies up to a few hundred MeV. Presently two implementations of this approach exist: Blann's Monte Carlo version of ALICE [7–9], and Chadwick's double differential hybrid Monte Carlo simulation (DDHMS) [8–12] code. In this paper we have tested the accuracy and ability of the latest version of Blann's code, ALICE2014, to predict neutron emission cross sections in heavy-ion reactions [13].

In order to understand the role of pre-equilibrium emission, we also compared our results with the Projection Angular Momentum Coupled Evaporation (PACE4) statistical model code [14] commonly used in calculating spectra of particles in heavy-ion-induced reactions. Since the PACE4 code does not take into account the pre-equilibrium and breakup processes, such a comparison is indicative of the pre-equilibrium components. Deviations between ALICE2014 and PACE4 in regions of the spectra where pre-equilibrium effects are not expected to contribute significantly are indicative of other assumptions for a similar set of parameters used in the two codes. In addition to pre-equilibrium effects, neutron emission at low energies and forward angles also includes a contribution from breakup. The ALICE2014 calculations include breakup by using the Fermi statistics breakup model [15]. In this model, the densities of excited states are taken into account, and the microcanonical statistical multi-fragmentation model is used to describe the disintegration of highly excited fragments of nuclear reactions.

Interpretation of neutron spectra have the advantage of being independent of the Coulomb barrier in the exit channel; moreover, neutron emission cross sections are generally much

*Corresponding author: sk.mukherjee-phy@msubaroda.ac.in

larger than those for charged particle emission. However, the experimental measurement of neutron spectra could be more challenging, requiring careful consideration of background, scattering from surrounding materials, good beam collimation, crosstalk between detectors, and uncertainties arising from detector efficiency considerations.

In recent years a few measurements of neutron multiplicities were carried out using ^{16,18}O and ^{19}F as projectiles on some isotopes of Pt to study the shell closure effects [16–19]. Also, Ramachandran *et al.* [20] measured neutron, proton, and α-particle multiplicities for ^{28}Si + ^{175}Lu. Very recently, Sharma *et al.* [21] made experimental measurements with ^{12}C and ^{16}O on a few heavy targets. The motivation of our work is to look at the global prediction of pre-equilibrium and breakup effects without specific reference to level density enhancement near magic numbers.

In the present work we measured ^{19}F-induced neutron spectra for three targets, ^{51}V, ^{89}Y, and ^{181}Ta, spanning a wide mass range and four beam energies (130, 140, 145, and 150 MeV). The measurement was carried out over eight laboratory angles (25°, 42°, 58°, 74°, 95°, 111°, 127°, and 143°) spanning a wide angular range. Experimental details are given in Sec. II. Sections III and IV give brief details about the ALICE2014 and PACE4 calculations and present a comparison of the calculations with the experimental results. A number of interesting points arise from the comparison and these are discussed in Sec. V.

II. EXPERIMENTAL DETAILS

In the present experiment, a pulsed ^{19}F beam obtained from the Bhabha Atomic Research Centre–Tata Institute of Fundamental Research (BARC-TIFR) Pelletron-LINAC facility, Mumbai, was utilized. The pulsed beam had a two-bunch structure with a time of 106.67 ns between bunches. Beam current in the range 1–3 pnA were used. All the targets were rolled from spectroscopic grade material to thicknesses in the range 1.5−1.8 mg/cm^2. Target thicknesses were determined by accurate weighing with a micro-balance. Targets were checked for impurities using the x-ray fluorescence technique.

Fourteen liquid scintillator neutron detectors (NE213) were used to cover the angular range 25°−143°. The time-of-flight (TOF) distances were in the range 65–82 cm. Special care was taken to reduce the background from the scattered neutrons. The beam dump, 1.5 m downstream, was shielded with concrete blocks. No beam line collimators near the target were used. The beam focusing and steering were periodically checked to ensure low background from the target frame. The background estimations were done using a blank target and shadow bar technique.

The Linux Advanced Multi-Parameter System–VERSA-Module Euro card (LAMPS-VME) [22] data acquisition system was used, triggered by an OR condition from the individual detectors qualified by beam RF signal. For each detector, TOF, pulse-shape discrimination (PSD) and anode signal amplitudes were recorded. The trigger logic ensured that the next master gate was blocked while the VME modules were busy. Dead time was deduced from scalars which counted raw master gates and blocked master gates. The detector efficiencies were obtained by making the measurements with a ^{252}Cf source on a thin (0.5 mm) stainless steel disk, kept at the target position enclosed in a small 4π ionization chamber detecting fission fragments. In this case TOF was measured with respect to fission fragments. Comparison was made with the efficiency curve of the neutron detector as a function of neutron energy obtained by using the Monte Carlo computer code (NEFF) [23]. The detector thresholds in the code were adjusted to match the experimental results. The neutron spectrum from ^{252}Cf is well known and its shape has been parametrized [24]. An overall agreement between the simulation results and the measured efficiencies was obtained (Fig. 1).

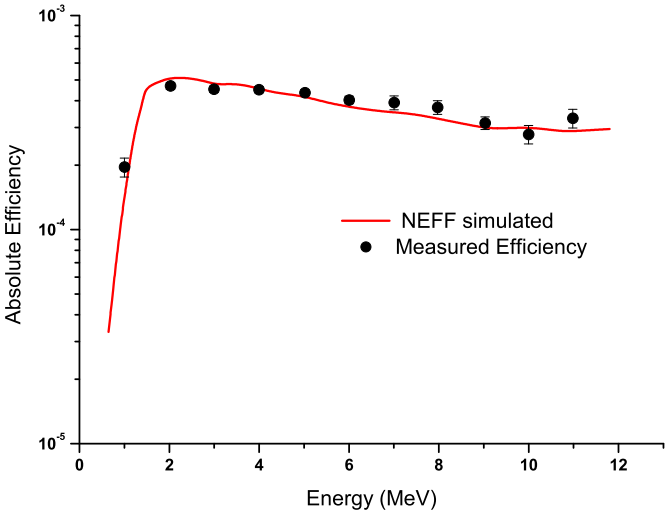

FIG. 1. Comparison of the experimentally obtained neutron efficiency (solid circles) with the same obtained using Monte Carlo simulation code NEFF (solid line).

The neutron energy spectra were obtained by converting TOF to energy on an event-by-event basis using the LAMPS program. Normalization was done in terms of target thickness (which was carefully measured), beam charge (from a calibrated current integrator), and detector efficiencies. TOF calibration was done by matching the distance between the 2 γ peaks to the beam bunch separation (106.67 ns). The graphical cuts were applied in the two-dimensional spectrum to select the neutrons. This is a polygonal gate in the two-dimensional spectrum of time of flight versus pulse-shape discrimination signal used to distinguish neutrons from gamma rays. A typical two-dimensional plot of TOF vs. PSD is given in Fig 2. This figure shows a clear separation between neutron and γ radiation. In the figure, the γ rays correspond to smaller values of the TOF and the PSD signals. The measured spectra were normalized using the simulated efficiencies over the energy range 1.5–17 MeV.

The estimated errors in the present measurement include statistical error and systematic errors arising from estimating target thickness, integrated beam current, and detector efficiency. The overall error in the present measurement was in the range 8–10%. These errors are shown in Figs. 3–14. These estimated errors are smaller than the experimental scatter point size.

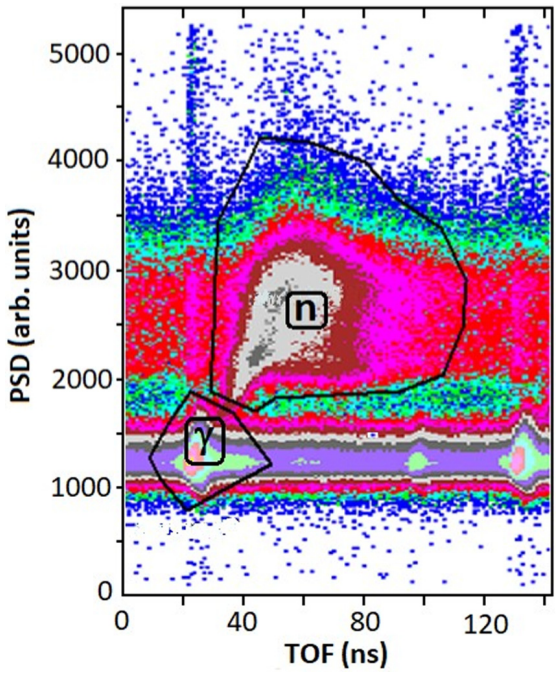

FIG. 2. Typical plot of pulse shape discrimination (PSD) signal versus time-of-flight (TOF) signal.

III. DETAILS OF ALICE2014 CALCULATIONS

The ALICE2014 code principally uses Monte Carlo simulations of the geometry-dependent hybrid (GDH) model for pre-equilibrium calculations and Weisskopf-Ewing evaporation for the equilibrium emission part.

It uses the fact that the three-exciton configuration produced by the interaction of a nucleon with a nucleus in a two-body process should give approximately the nucleon energy distribution represented by the three-exciton density function. The angular distribution calculations are done using the Chadwick-Oblozinsky linear momentum conservation model [10,11]. In the Monte Carlo approach [7], each successive scattering of a nucleon is treated as producing a new three-exciton configuration, consistent with the two-body assumption. This avoids use of the higher order exciton densities which were inconsistent with population by a two-body mechanism [25]. This Monte Carlo approach can be used to calculate multiplicities of pre-compound emitted nucleons. In other words, the Monte Carlo approach allows more than one emission of pre-equilibrium ejectiles (so-called multiple pre-equilibrium).

For nearly four decades, the GDH model proposed by Blann [26] has been used successfully for the modeling of non-equilibrium particle and light cluster emission in nuclear reactions induced by intermediate energy particles. In the GDH

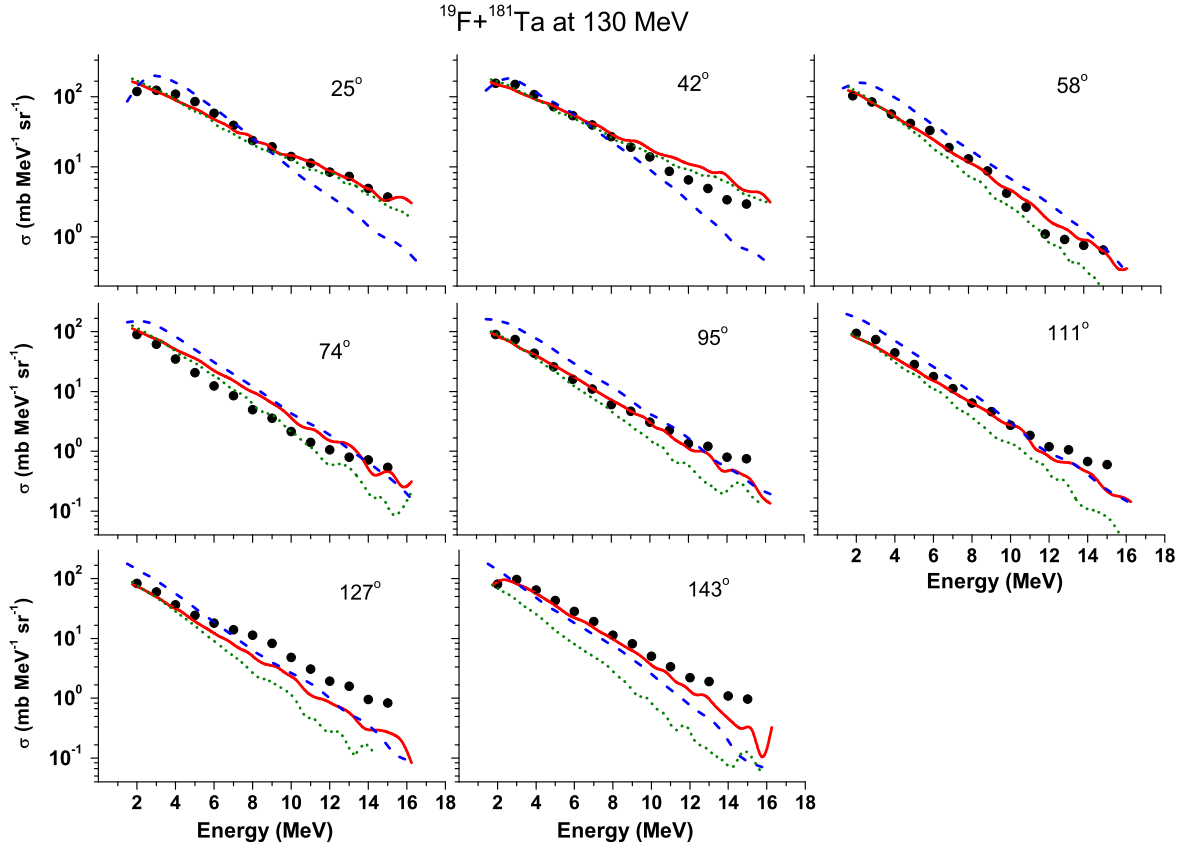

FIG. 3. Neutron emission differential cross sections for 130 MeV ^{19}F on ^{181}Ta target. The solid symbols are the experimental results of this work. The calculated cross sections are shown as a solid red curve (OB level density) and dash-dotted green curve (KRK level density) as obtained with the nuclear reaction code ALICE2014 and dashed blue curve as obtained from PACE4. The estimated errors are smaller than the experimental scatter point size.

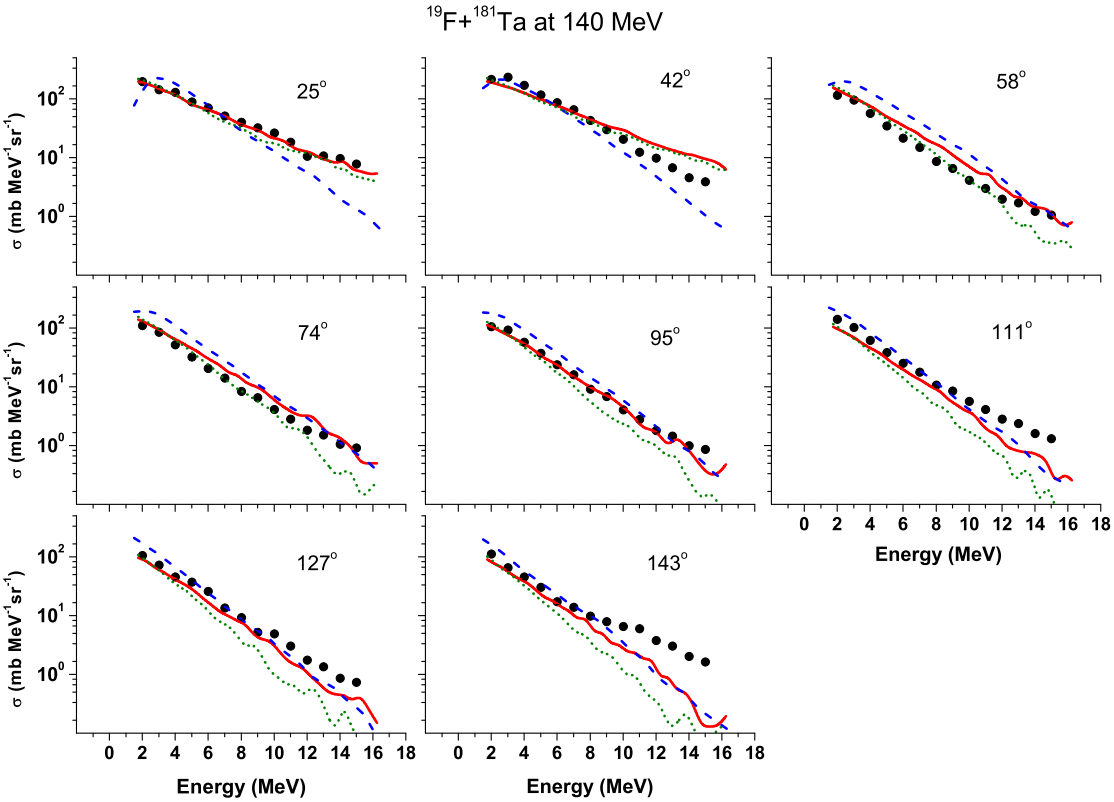

FIG. 4. Neutron emission differential cross sections for 140 MeV ^{19}F on ^{181}Ta target. The other details are the same as in Fig. 3.

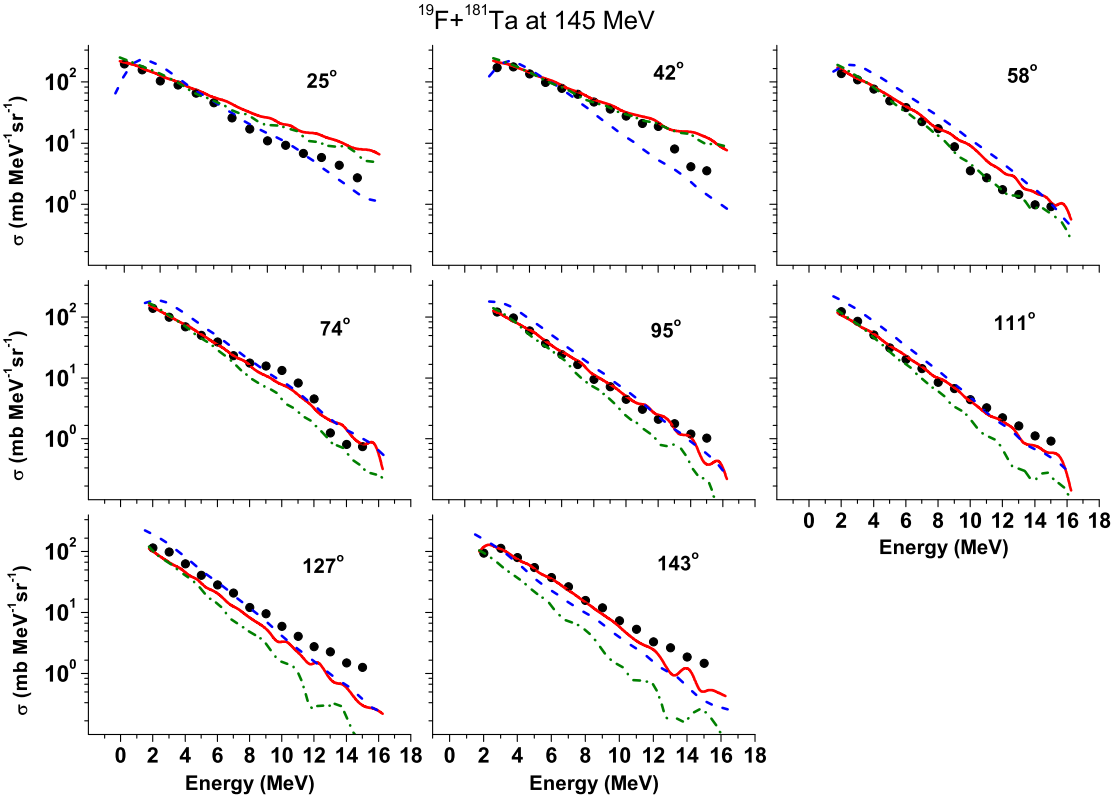

FIG. 5. Neutron emission differential cross sections for 145 MeV ^{19}F on ^{181}Ta target. The other details are the same as in Fig. 3.

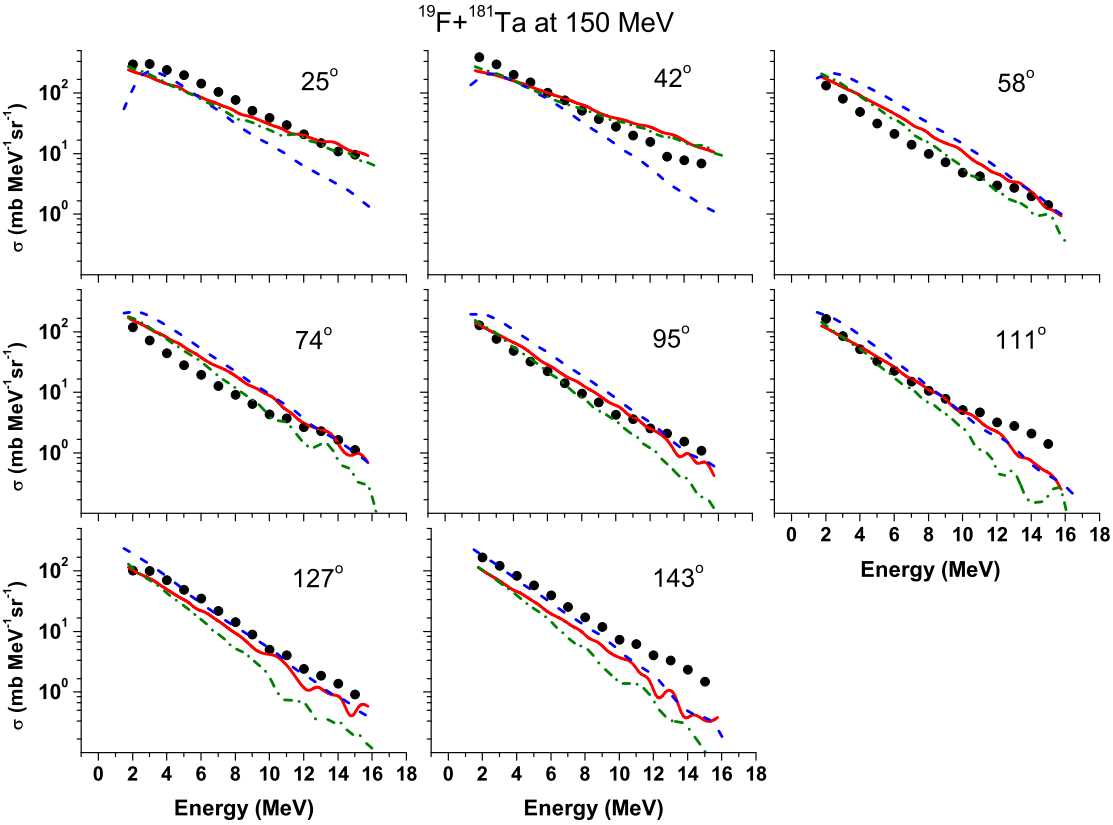

FIG. 6. Neutron emission differential cross sections for 150 MeV ^{19}F on ^{181}Ta target. The other details are the same as in Fig. 3.

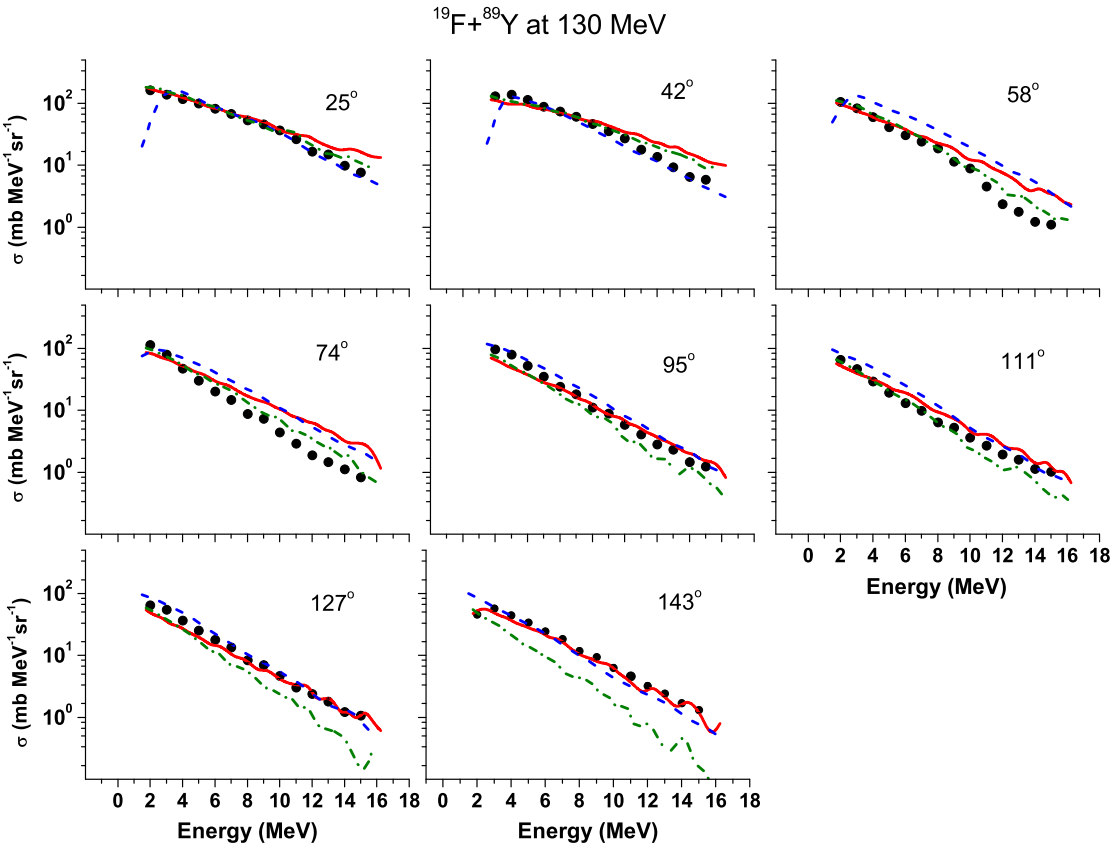

FIG. 7. Neutron emission differential cross sections for 130 MeV ^{19}F on ^{89}Y target. The other details are the same as in Fig. 3.

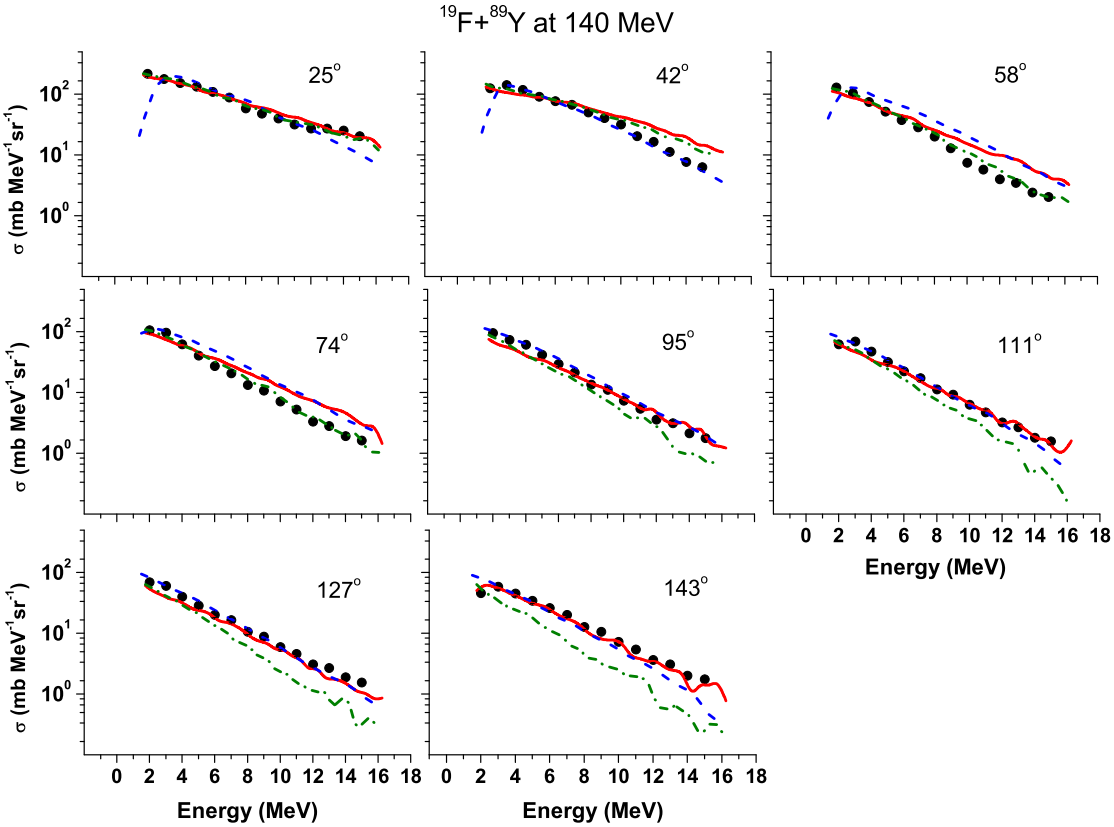

FIG. 8. Neutron emission differential cross sections for 140 MeV ^{19}F on ^{89}Y target. The other details are the same as in Fig. 3.

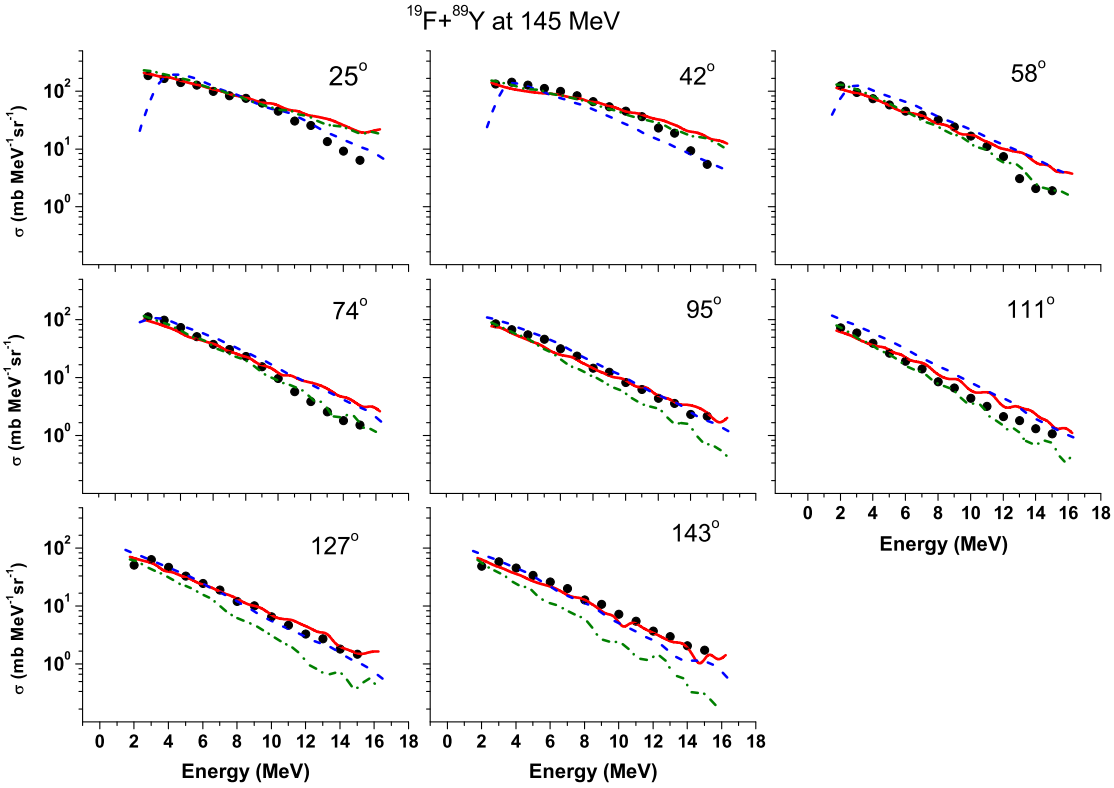

FIG. 9. Neutron emission differential cross sections for 145 MeV ^{19}F on ^{89}Y target. The other details are the same as in Fig. 3.

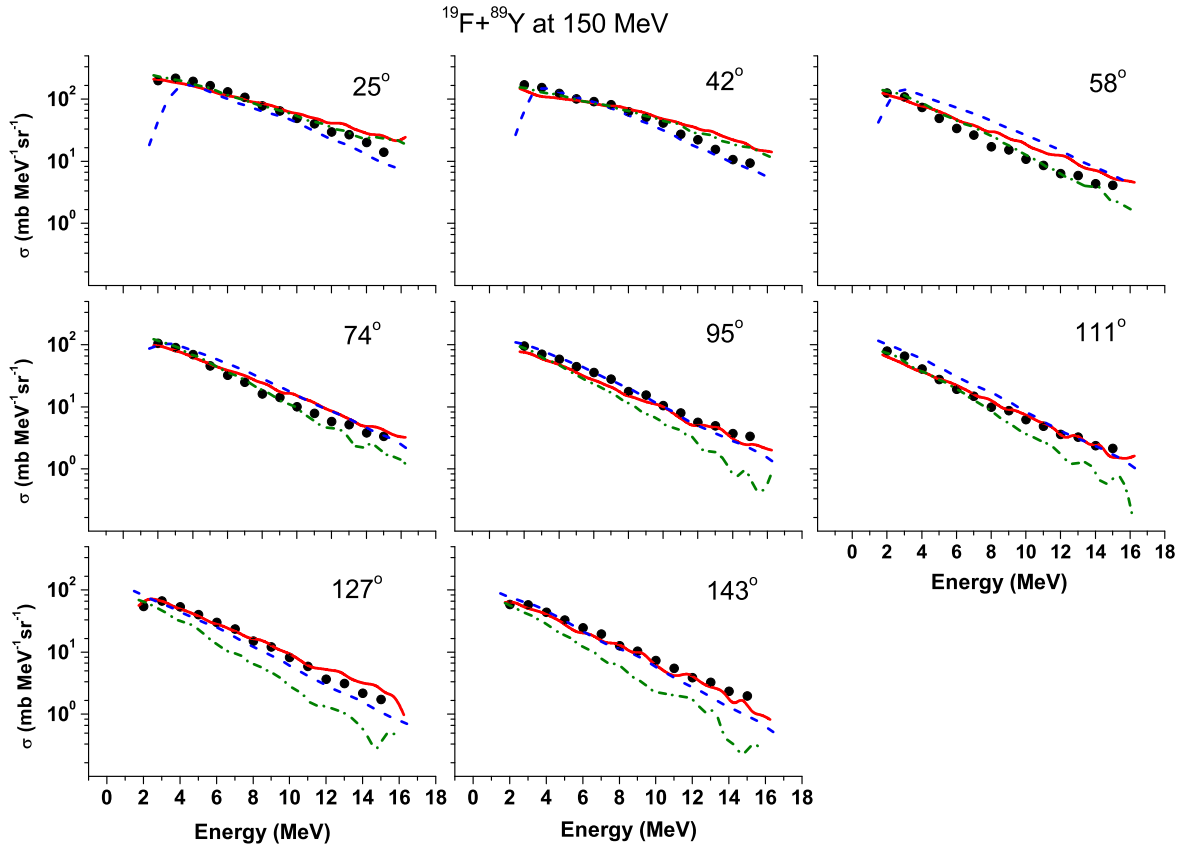

FIG. 10. Neutron emission differential cross sections for 150 MeV ^{19}F on ^{89}Y target. The other details are the same as in Fig. 3.

model the pre-equilibrium energy distribution of nucleons is calculated as follows:

$$\frac{d\sigma}{d\varepsilon_x} = \pi\lambda\!\!\!^{-2} \sum_{l=0}^{\infty}(2l+1)T_l \times \sum_{n=n_0} X_x^n \frac{\omega(\mathrm{p}-1,\mathrm{h},U)}{\omega(\mathrm{p.h.}E)} \frac{\lambda_x^e}{\lambda_x^e+\lambda_x^+}\, g\, D_n, \quad (1)$$

where T_l is the transmission coefficient for the lth partial wave; X_x^n is the number of nucleons of type x in the n-exciton state; ε_x is the channel energy of the nucleon; $\omega(\mathrm{p.h.}E)$ is the density of exciton states with particles, p, and holes, h ($\mathrm{p}+\mathrm{h}=n$) at the excitation energy E; U is the final excitation energy, $U = E - Q_x - \varepsilon_x$, and Q_x is the nucleon separation energy; D_n is the "depletion" factor; and n_0 is the initial exciton number.

The nucleon emission rate λ_x^e is equal to [27]

$$\lambda_x^e = \frac{(2S_x+1)\mu_x\varepsilon_x\sigma_x^{\mathrm{inv}}(\varepsilon_x)}{\pi^2\lambda\!\!\!^{-3}g_x},$$

where S_x and μ_x are the spin and reduced mass of the outgoing nucleon of type x, σ_x^{inv} is the inverse reaction cross section for particle x, and g_x is the single-nucleon state density.

The l-dependent intra-nuclear transition rate λ_x^+ is calculated using the nucleon-nucleon scattering cross section corrected for the Pauli principle and the average nuclear matter density at the distance from $l\lambda\!\!\!^{-}$ to $(l+1)\lambda\!\!\!^{-}$. For nucleon-induced reactions the density of excited states with the number of excitons with $n = 2$ and 3 is obtained considering the finite depth of the nuclear potential well. The number of nucleons of x type in the n-exciton state X_x^n is calculated using the ratio of the nucleon-nucleon cross sections obtained by taking into account the Pauli principle and the nucleon motion. Multiple pre-compound nucleon emission is simulated by means of Monte Carlo simulation.

Equilibrium emission was calculated according to the Weisskopf-Ewing (WE) model [28] neglecting angular momentum. In the evaporation model, the basic parameters are binding energies, inverse reaction cross section, the pairing, and the level-density parameters. The reaction cross section for incident channel a and exit channel b can be written as

$$\sigma_{ab}^{\mathrm{WE}} = \sigma_{ab}(E_{\mathrm{inc}})\frac{\Gamma_b}{\sum_{b'}\Gamma_{b'}},$$

where E_{inc} is the incident energy. Γ_b is expressed as

$$\Gamma_b = \frac{2s_b+1}{\pi^2\hbar^2}\mu_b\int \sigma_b^{\mathrm{inv}}(\varepsilon)\varepsilon\frac{\omega_1(U)}{\omega_1(E)}\,d\varepsilon,$$

where U, μ_b, and s_b are the excitation energies, the reduced mass, and the spin of the residual nucleus, respectively. $\sigma_b^{\mathrm{inv}}(\varepsilon)$ is the inverse reaction cross section. $\omega_1(E)$ is the total single-particle level density which is given by

$$\omega_1(E) = \frac{1}{\sqrt{48}}\frac{\exp[2\sqrt{\alpha(E-D)}]}{E-D}, \quad \alpha = \frac{6}{\pi^2}g.$$

The calculations using this code have been done without parameter adjustment by selecting the Obninsk (OB) [29] as well as Kataria-Ramamurthy-Kapoor (KRK) level-density

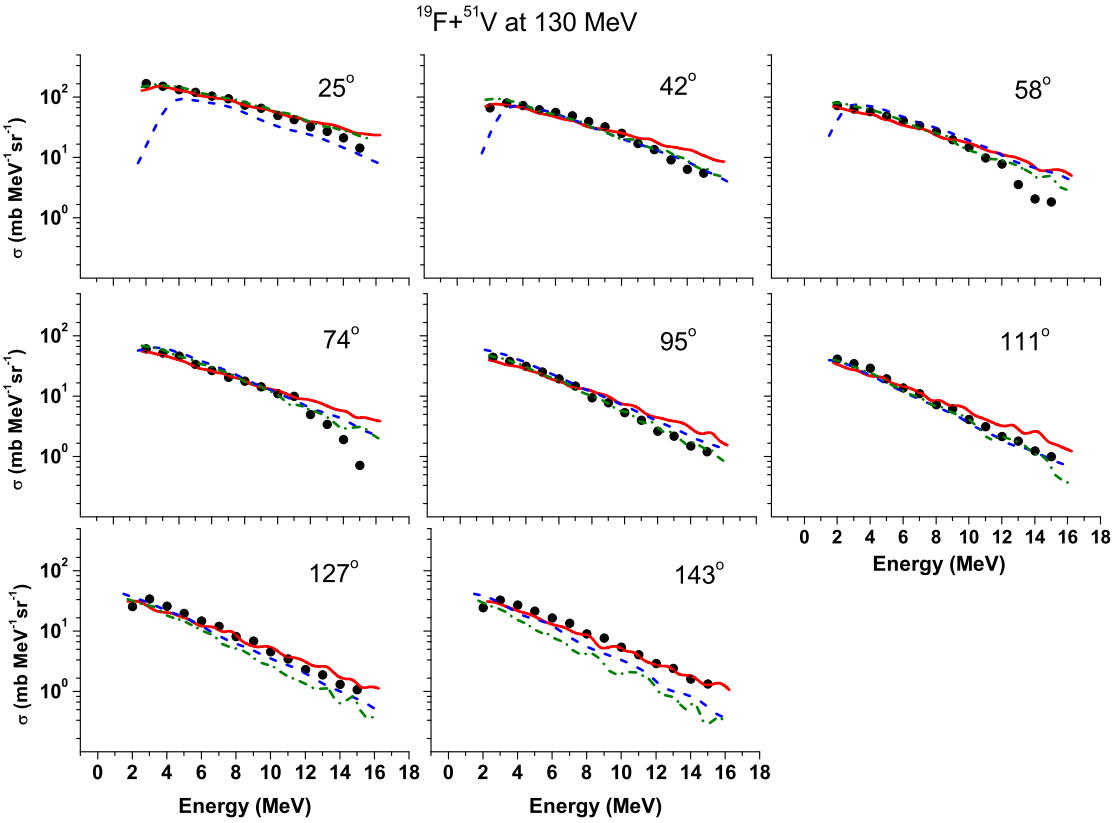

FIG. 11. Neutron emission differential cross sections for 130 MeV ^{19}F on ^{51}V target. The other details are the same as in Fig. 3.

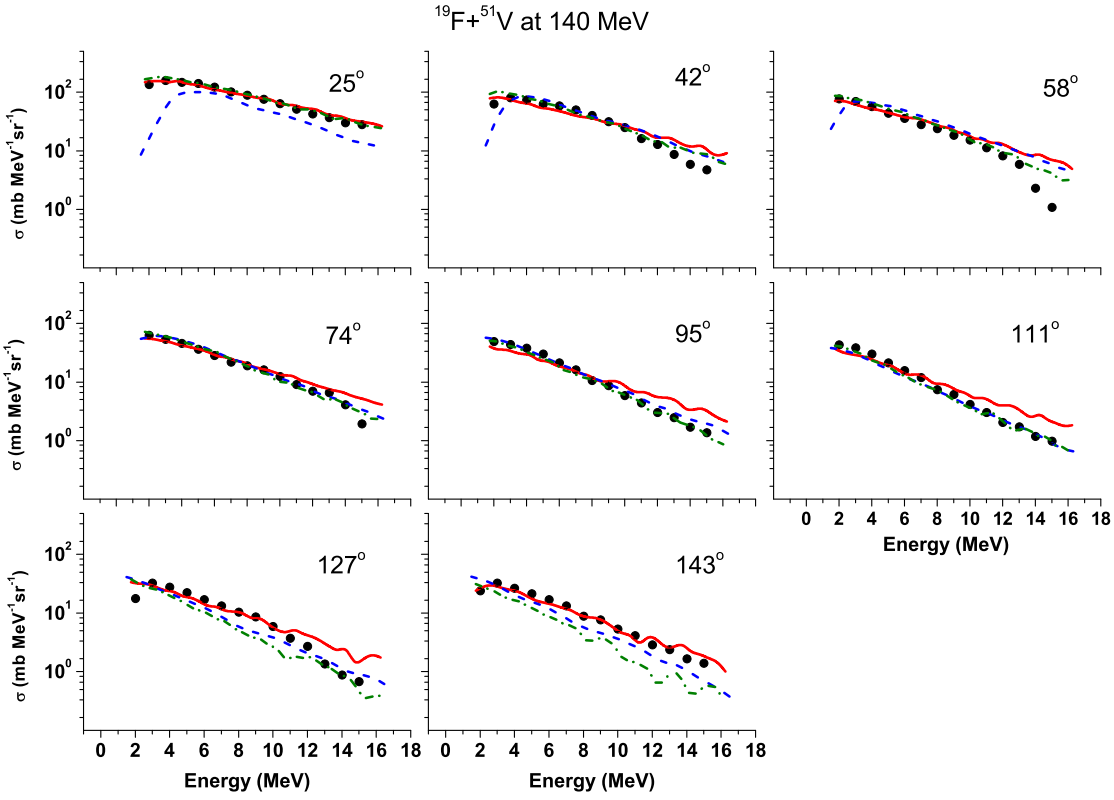

FIG. 12. Neutron emission differential cross sections for 140 MeV ^{19}F on ^{51}V target. The other details are the same as in Fig. 3.

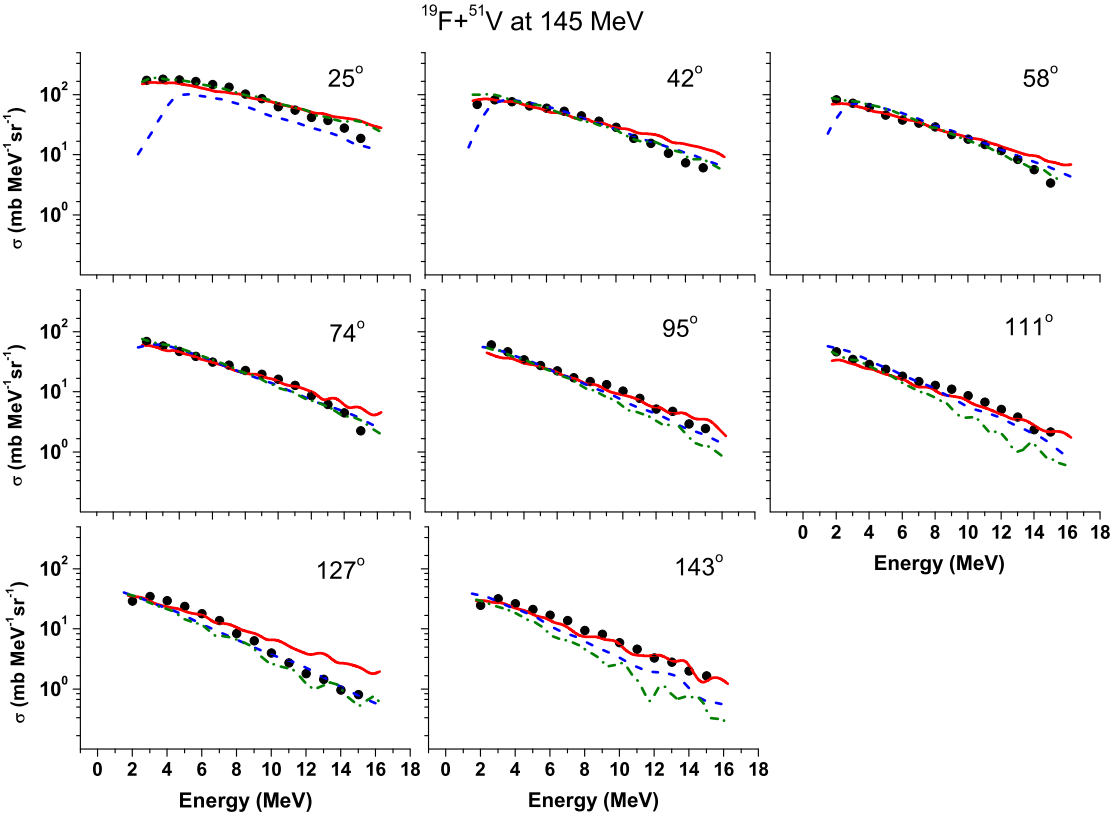

FIG. 13. Neutron emission differential cross sections for 145 MeV ^{19}F on ^{51}V target. The other details are the same as in Fig. 3.

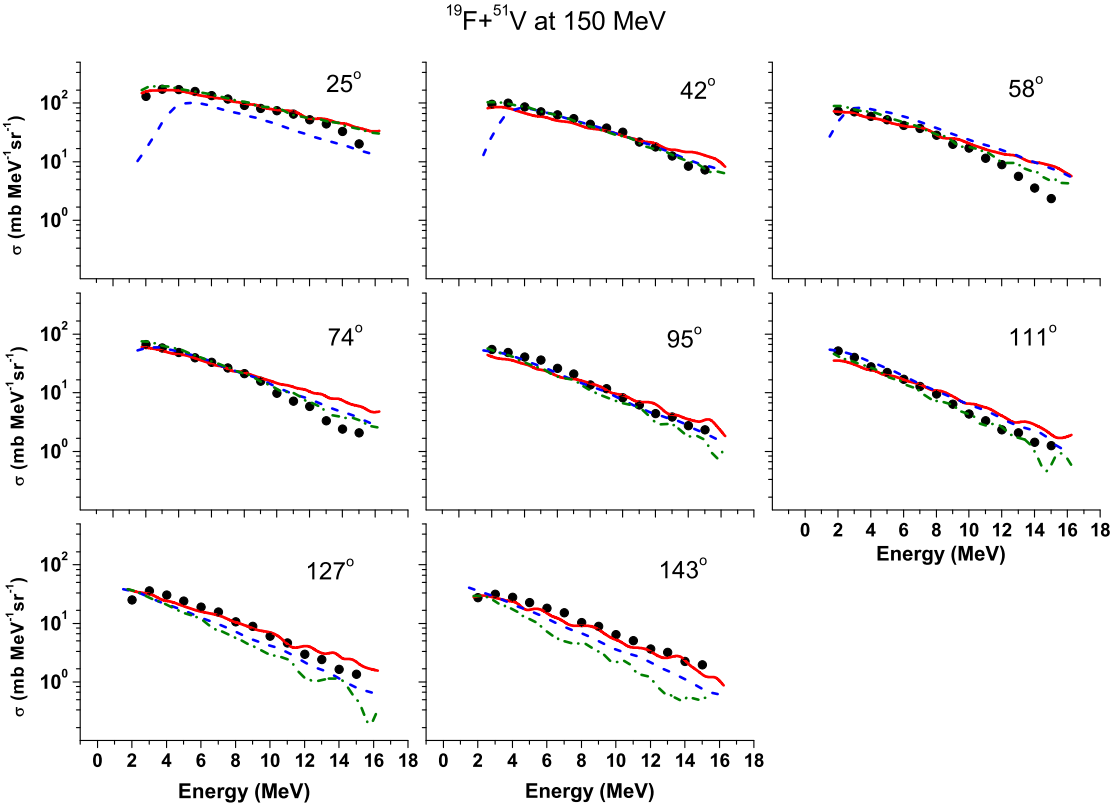

FIG. 14. Neutron emission differential cross sections for 150 MeV ^{19}F on ^{51}V target. The other details are the same as in Fig. 3.

options [30]. The OB level-density option gives a better reproduction of our data as compared to KRK level density and other options [30,31]. Comparisons of the experimental results with ALICE2014 calculations are given in Figs. 3–18.

IV. DETAILS OF PACE4 CALCULATION

The statistical model code Projection Angular-Momentum Coupled Evaporation (PACE4) uses a Monte Carlo procedure to determine the decay sequence of an excited nucleus using the Hauser-Feshbach formalism. Sequential decays are considered until any further decay is prohibited due to the energy and angular momentum conservation laws. A random number selection determines the actual final state to which the nucleus decays and the process is then repeated for other cascades until all the nuclei reach the ground state. The transmission coefficients for light particle emission (n, p, α) are determined using optical model potentials [32,33]. The code also provides event-by-event traceback of the entire decay sequence from the compound nucleus into any one of the exit channels. The fusion cross sections are obtained from the Bass model [34]. The fission probability is calculated using the Bohr-Wheeler saddle point formalism [35]. The PACE4 code has the ability to provide information on energy and angular distributions of evaporated particles.

The partial cross section for CN formation at angular momentum (ℓ) and specific bombarding energy is given by

$$\sigma_l = \frac{\pi\lambda^2}{4\pi^2}(2l+1)T_l,$$

where λ is the reduced wavelength and T_l is the transmission coefficient given by

$$T_l = [1 + \exp(l - l_{\max})/\delta]^{-1},$$

where δ is the diffuseness parameter and $l_{\max}$ is determined by the total fusion cross section σ_F, and

$$\sigma_F = \sum_{l=0}^{\infty} \sigma_l$$

A comparison of the experimental results with the PACE4 calculations (dashed lines) is given in Figs. 3–18.

V. DISCUSSION AND CONCLUSIONS

A comparison of the results with the calculations reveals that the ALICE2014 code is fairly successful in predicting the angle-dependent spectra globally for all the targets without any parameter adjustment. We used both OB and KRK level density in our calculations. Results using the KRK level density were somewhat inferior. In another work [6] we also concluded that the OB level density with the ALICE2014 model works well, whereas the results with KRK level density are not as good. The PACE4 calculations were done with the Fermi gas level density using the level density parameter $a = A/10\,\mathrm{MeV}^{-1}$.

Figures 3–14 (angle-dependent energy spectra), Figs. 15–17 (energy-dependent angular distributions at 150 MeV beam energy), and Fig. 18 (energy integrated angular distribution at 150 MeV beam energy) show a comparison of calculated results with the measured data. The ALICE2014 code is fairly

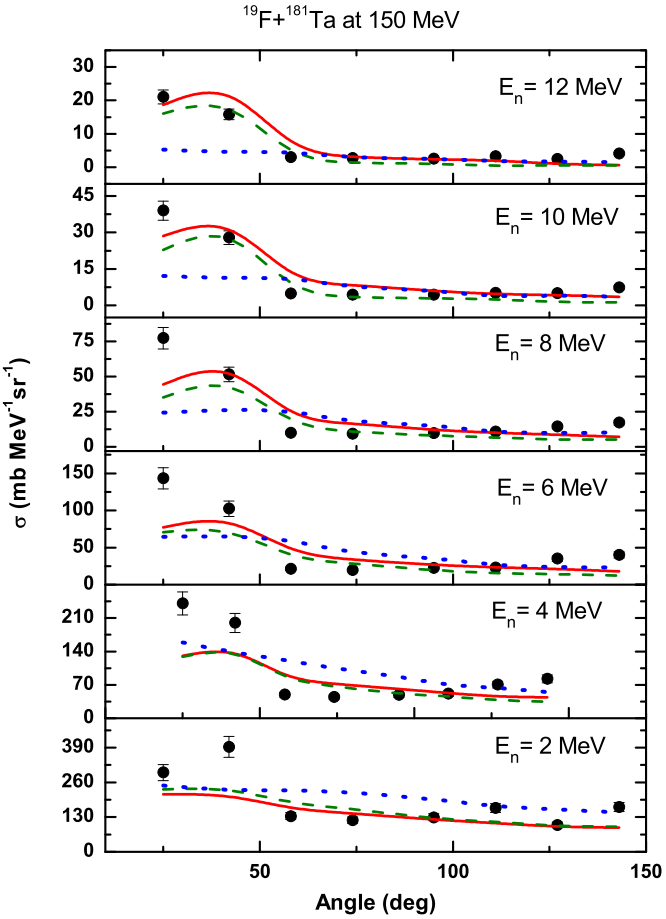

FIG. 15. Neutron angular distribution at various emission energies for ^{19}F (150 MeV) + ^{181}Ta. PACE4 (dotted blue curve), ALICE2014 (KRK) (dashed green curve), ALICE2014 (OB) (solid red curve), and present experimental results (solid black points with error bars).

successful in reproducing the results globally without any parameter adjustment. The OB level density was found to give better results than the KRK level density. This was also the case in an earlier work [6].

PACE4 calculations were done with the Fermi gas level density using the level density parameter $a = A/10\,\mathrm{MeV}^{-1}$. The low neutron energy region (below approximately 8 MeV) is dominated by statistical evaporation, while at higher neutron energies, the contribution of pre-equilibrium emission and breakup and related processes are expected to be large, especially at the highest beam energy. At low energies also there may be a contribution of the breakup reaction, which is not included in PACE4. In ALICE2014 breakup is included in an approximate way [13,15]. Both contributions are forward peaked; however, pre-equilibrium emission increases for higher neutron energies. Considering the overall picture first, Fig. 18, plotted only at the highest beam energy, clearly shows the forward peaked nature of the data, fairly well reproduced by ALICE2014. The PACE4 calculations tend to merge with ALICE2014 for angles greater than 100°.

More details can be seen from the angle-dependent energy spectra. Considering the spectra at the most forward angles,

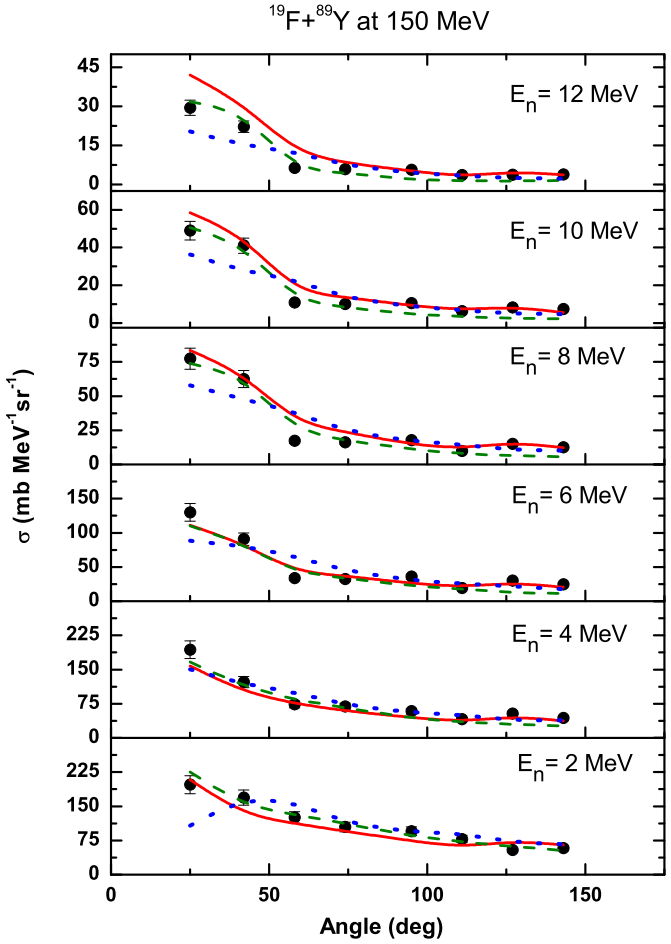

FIG. 16. Neutron angular distribution at various emission energies for ^{19}F (150 MeV) + ^{89}Y. The other details are the same as in Fig. 15.

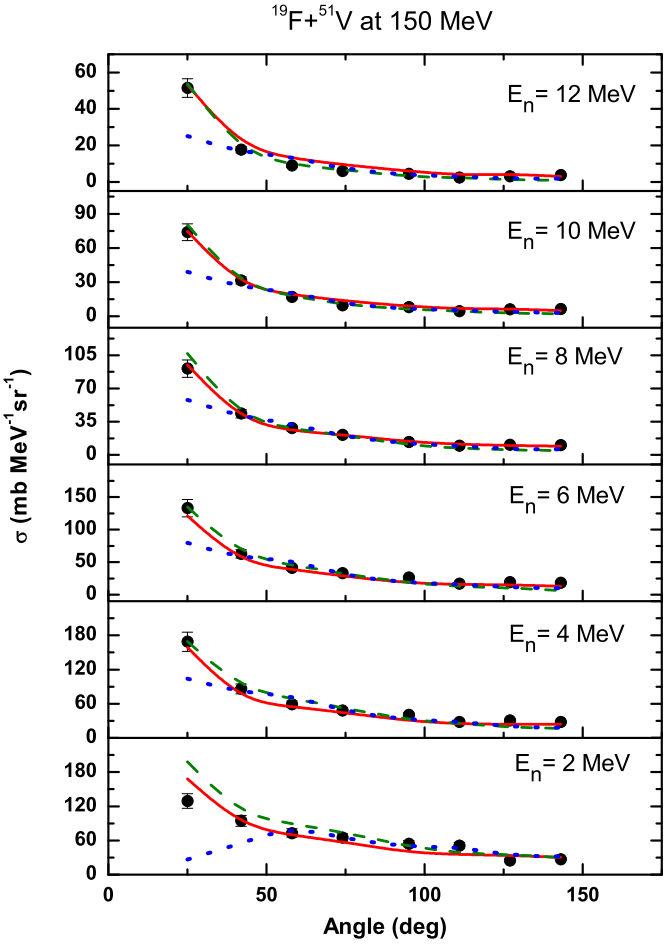

FIG. 17. Neutron angular distribution at various emission energies for ^{19}F (150 MeV) + ^{51}V. The other details are the same as in Fig. 15.

PACE4 calculations are lower than ALICE2014 calculations at higher neutron emission energies. The difference is greater for higher projectile energies and is more for ^{181}Ta as compared to ^{89}Y and ^{51}V. The experimental trend is in favor of ALICE2014 calculations for the ^{181}Ta target; however, for ^{89}Y and ^{51}V targets the data for high neutron energies fall in between the ALICE2014 and PACE4 predictions. Similarly, at the most forward angles and at the lowest neutron energies, PACE4 predictions are underestimated as compared to the data, while ALICE2014 predictions approximately reproduce the data. At these forward angles the breakup contribution is expected to be high. At intermediate angles around 90°–100°, ALICE2014 and PACE4 calculations are fairly close for all the targets and the experimental measurements are well predicted by both calculations. Here the contribution from breakup and pre-equilibrium are supposed to be small.

It is interesting to examine the spectra at 25°. In all the cases, it is observed that there is a fall in the PACE4 calculations at low (below 2 MeV) as well as at high energies. The effect is most pronounced at the highest beam energy. Deviations at lower neutron energy may be due to breakup or another reaction mechanism such as transfer and this is expected to be higher for heavier targets. At high neutron energy the pre-equilibrium effect may also become important, as evident from the reasonably good agreement shown by the ALICE2014 predictions. Pre-equilibrium emission is expected to be more in the heavy-mass target (^{181}Ta) as compared to the light- and medium-mass targets (^{51}V and ^{89}Y) and increases with beam energy. Breakup is expected to be higher for heavier targets; however, the fall of PACE4 cross sections at 25° for the lowest neutron energies are stronger for lighter targets, being strongest for the ^{51}V target where a fall can also be observed around the region of 42°, indicating that breakup or something other than breakup might also be playing a role.

At the most backward angle at high emission energies, the reproduction of data for the ^{181}Ta target is not as good. Considering the ^{181}Ta target, at beam energy 130 MeV, the PACE4 calculation falls off faster than the ALICE2014 calculation, but the experimental data are somewhat higher than the ALICE2014 prediction. At a beam energy of 150 MeV, the two calculations are similar in trend, but the measured data are higher. Considering the ^{89}Y target, the data are in agreement with ALICE2014 but the PACE4 calculations fall off only slightly faster. In the case of the ^{51}V target, the data clearly favor the ALICE2014 calculations, which are substantially higher than the PACE4 calculations at higher neutron energies. Thus, it appears

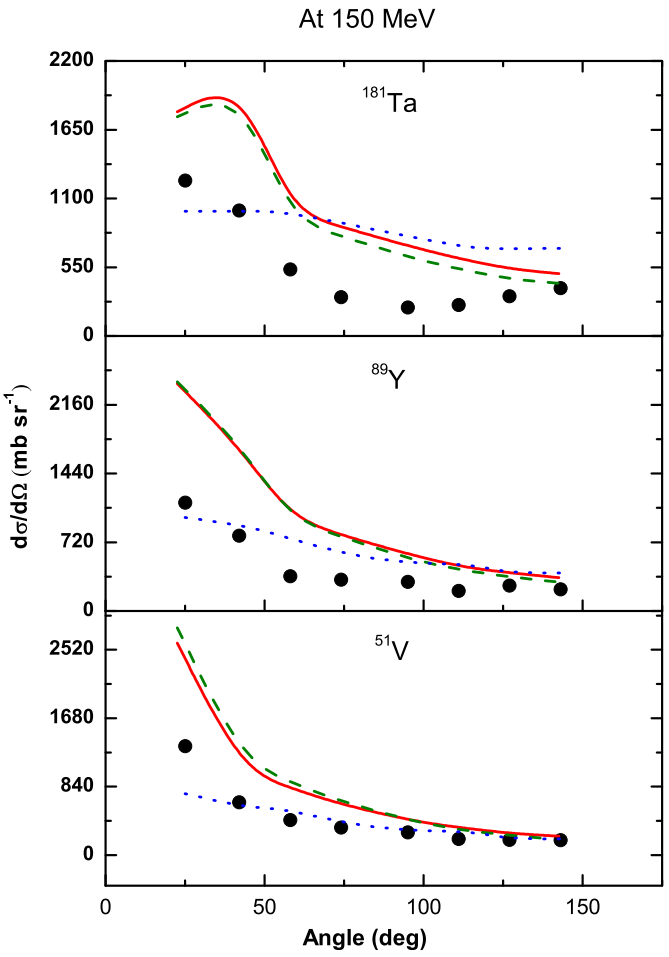

FIG. 18. The energy integrated angular distribution for emitted neutrons for various targets at 150 MeV beam energy. The other details are the same as in Fig. 15.

that there may be pre-equilibrium effects which cause more neutron emission at higher energies, even at 143°. This is not predicted by the ALICE2014 calculation for the heaviest target but is correctly predicted for the lightest target.

The above observations can be further clarified from angular distribution plots for ^{19}F + ^{181}Ta, ^{89}Y, and ^{51}V systems at the highest beam energy of 150 MeV (Figs. 15 –17). In the case of a heavy (^{181}Ta) system (Fig. 15), there is a considerable amount of pre-equilibrium neutron emission at higher neutron energies as expected in the heavy targets. However, in this system, the ALICE2014 calculations slightly underpredict the data. At the lowest neutron energies, ALICE2014 also underpredicts the experimental results. It can be clearly observed that for the medium (^{89}Y) (Fig. 16) and light (^{51}V) (Fig. 17) systems with the increase of emitted neutron energies, there is a considerable gap between the PACE4 and ALICE2014 results at forward angles less than 50°. PACE4 calculations grossly underestimate the experimental results in this region. The close agreement between experimental results and ALICE2014 prediction at all the neutron energies may be an indication of breakup and/or pre-equilibrium emission. At backward angles, greater than 50°, both PACE4 and ALICE2014 reproduce the experimental results, thereby indicating an absence of pre-equilibrium and breakup. At most backward angles at high emission energies, the reproduction of data is not as good for the ^{181}Ta target. In Fig. 18 the failure of ALICE2014 for the ^{181}Ta target at 25° is worth attention. This could be a shortcoming of the simplified breakup model used in the ALICE2014 predictions [15]. This figure also brings out the dependence of the combined breakup and pre-equilibrium effect as a function of target mass.

In summary, we made an experimental measurement of neutron spectra in ^{19}F-induced reactions for three targets. The trend of the data is well reproduced by ALICE2014 calculations. A comparison with PACE4 calculations, which includes only statistical evaporation, brings out the contributions arising from breakup and pre-equilibrium effects. Both arise at forward angles; however, the former contributes to the low-energy part of the spectra, while the latter contributes at higher neutron energies. While calculations using the ALICE2014 model with OB level densities reproduce the data globally quite well, a few shortcomings have been pointed out. It may be remarked cautiously that the breakup comes at lower neutron energies and forward angles while pre-equilibrium comes at high neutron energies and forward angles. PACE does not include breakup. In our graphs it is seen in the low-energy part of the spectra that PACE underestimates while ALICE2014 does better. This may be because the breakup of light particles is included in the ALICE2014 code. From the present study it may also be concluded that the target mass dependence on the reaction mechanism cannot be ignored. Some shortcomings of the ALICE2014 calculations are also brought out.

ACKNOWLEDGMENTS

One of the authors (S.M.) thanks the Department of Atomic Energy, Board of Research in Nuclear Sciences (DAE-BRNS), Mumbai, India, for the sanction of a major research project (Sanction No. 36(6)/14/22/2016-BRNS). The authors are grateful to the staff of the BARC-TIFR Pelletron Accelerator Facility. G.F.S. thanks the Radiation Safety Information Computational Centre, Oak Ridge National Laboratory, USA, for providing the ALICE2014 code for the present theoretical analysis.

[1] M. Blann, Annu. Rev. Nucl. Sci. **25**, 123 (1975).
[2] J. J. Griffin, Phys. Rev. Lett. **17**, 478 (1976); Phys. Lett. B **24**, 5 (1967).
[3] E. Gadioli, Erba E. Gadioli, J. J. Hogan, and K. I. Burns, Z. Phys. A **301**, 289 (1981).
[4] H. Feshbach, A. Kerman, and S. Koonin, Ann. Phys. **125**, 429 (1980).
[5] R. Bonetti, M. Camnasio, L. Colli Milazzo, and P. E. Hodgson, Phys. Rev. C **24**, 71 (1981).
[6] J. Acharya, S. Mukherjee, G. F. Steyn, N. L. Singh, and A. Chatterjee, Phys. Rev. C **93**, 024608 (2016).
[7] M. Blann, Phys. Rev. C **54**, 1341 (1996).
[8] M. Blann and M. B. Chadwick, Phys. Rev. C **57**, 233 (1998).
[9] M. Blann and M. B. Chadwick, Phys. Rev. C **62**, 034604 (2000).

[10] M. B. Chadwick and P. Oblozinsky, Phys. Rev. C **46**, 2028 (1992).
[11] M. B. Chadwick and P. Oblozinsky, Phys. Rev. C **50**, 2490 (1994).
[12] L. Brito and B. V. Carlson, EPJ Web Conf. **69**, 00024 (2014).
[13] M. Blann and A. Y. Konobeev, Pre-compound cluster decay in HMSALICE (unpublished), available in documentation supplied with RSICC code package PSR-550 (package name: ALICE 2014/ALICE 2017), https://rsicc.ornl.gov /codes /psr/psr5/psr-550.html.
[14] A. Gavron, Phys. Rev. C **21**, 230 (1980).
[15] B. V. Carlson *et al.*, J. Phys.: Conf. Ser. **312**, 082017 (2011).
[16] V. Singh *et al.*, Phys. Rev. C **87**, 064601 (2013).
[17] R. Sandal *et al.*, Phys. Rev. C **87**, 014604 (2013).
[18] V. Singh *et al.*, Phys. Rev. C **86**, 014609 (2012).
[19] F. Gramegna *et al.*, J. Phys.: Conf. Ser. **580**, 012011 (2015).
[20] K. Ramachandran, A. Chatterjee, A. Navin, K. Mahata, A. Shrivastava, V. Tripathi, S. Kailas, V. Nanal, R. G. Pillay, A. Saxena, R. G. Thomas, S. Kumar, and P. K. Sahu, Phys. Rev. C **73**, 064609 (2006).
[21] M. K. Sharma *et al.*, Phys. Rev. C **91**, 014603 (2015).
[22] http://www.tifr.res.in/∼pell/lamps.html.
[23] G. Dietze and H. Klein, Report No. PTB-ND-22. Physikalisch-Technische Bundesanstalt, Braunschweig, Germany (1982), https://inis.iaea.org/search/search.aspx?orig_q=RN:14769159.
[24] D. G. Madland and J. R. Nix, in *Proceedings of the Conference on Nuclear Data for Science and Technology*, edited by K. H. Bockhoff (D. Reidel Publishing Company, Dordrecht, Holland, 1983), p. 473.
[25] J. Bisplinghoff, Phys. Rev. C **33**, 1569 (1986).
[26] M. Blann, Phys. Rev. Lett. **28**, 757 (1972).
[27] M. Avrigeanu and V. Avrigeanu, IAEA0971, NEA Data Bank (1996).
[28] V. F. Weisskopf and D. H. Ewing, Phys. Rev. **57**, 472 (1940).
[29] A. V. Ignatyuk, J. L. Weil, S. Raman, and S. Kahane, Phys. Rev. C **47**, 1504 (1993).
[30] S. K. Kataria, V. S. Ramamurthy, and S. S. Kapoor, Phys. Rev. C **18**, 549 (1978); **19**, 297 (1979).
[31] A. Gilbert and A. G. W. Cameron, Can. J. Phys. **43**, 1446 (1965).
[32] C. M. Perey and F. G. Perey, At. Nucl. Data Tables **17**, 1 (1976).
[33] J. R. Huizenga and G. Igo, Nucl. Phys. **29**, 462 (1962).
[34] R. Bass, Phys. Rev. Lett. **39**, 265 (1977).
[35] N. Bohr and J. A. Wheeler, Phys. Rev. **56**, 426 (1939).

Available online at www.sciencedirect.com

ScienceDirect

Nuclear Physics A 996 (2020) 121695

NUCLEAR PHYSICS A

www.elsevier.com/locate/nuclphysa

Non-equilibrium emission of alpha particles in the interaction of ^{14}N with ^{59}Co and ^{93}Nb at incident energy of 250 MeV

J. Acharya [a,*], S. Mukherjee [a,*], G.F. Steyn [b], S.V. Förtsch [b], F.D. Smit [b], R.T. Newman [b], J.J. Lawrie [b], O.V. Fotina [c], A. Chatterjee [a]

[a] *Department of Physics, Faculty of Science, The M.S. University of Baroda, Vadodara 380020, India*
[b] *iThemba LABS, National Research Foundation, PO Box 722, Somerset West, South Africa*
[c] *Physics Department, SINP, M.V. Lomonosov Moscow State University, Moscow, Russian Federation*

Received 7 August 2019; received in revised form 25 November 2019; accepted 6 January 2020
Available online 10 January 2020

Abstract

In this work, the results of measured inclusive double differential cross sections of α particles emitted in the interaction of ^{14}N with ^{59}Co and ^{93}Nb at incident energy of 250 MeV are presented. The experimental data were collected in a wide angular range from 8 to 100 degrees in the laboratory system. The analysis of these data suggests that the measured alpha spectra contains contributions of alpha particles originating from various reaction mechanisms, all of which are important at this high energy. We have also compared our experimental results with the calculations by using a recently developed theoretical model code. This recently developed pre-equilibrium model code is hereby put to a stringent test as to how it performs in case of heavy ion reactions at such high energies.

Keywords: Preequilibrium emission; Heavy ion reaction; Direct reactions; α-Particle spectra; PACE4

* Corresponding authors.
E-mail addresses: jaimin.acharya-padra@msubaroda.ac.in (J. Acharya), sk.mukherjee-phy@msubaroda.ac.in (S. Mukherjee).

https://doi.org/10.1016/j.nuclphysa.2020.121695

1. Introduction

At the projectile energies of 200 MeV and above, heavy ion induced pre-equilibrium emission of nucleons, light charged particles and evaporation residues presents a challenge towards our understanding of physics involving heavy ion reaction mechanism [1]. Efforts have been made in past to identify and predict the reaction cross-section for dominant reaction mechanisms that leads to the emission of nucleons, alpha and other light particles. It is well established that in heavy ion reactions, the compound nucleus mechanism is competing with non-equilibrium and direct reaction processes which are even more dominant at high energies. Experiments have clearly indicated that in such non-equilibrium and direct reactions, alpha particles comprise a major contribution to the emission cross section of all the outgoing particles [2]. Most of these alpha particles originate from projectile break-up [3]. It is possible to separate out and estimate the contributions from direct and evaporation processes from angular distribution and energy spectra. For the case of nucleon emission there are consistent theoretical approaches available which provides a good account of experimental data over a wide range of incident energy and target-mass region [4]. The theoretical model code developed by E. Gadioli, et al. [5] was able to predict the contribution of different reaction mechanism involved quite well. There are very few theoretical codes available which addresses the domain of non-equilibrium emission of alpha particles in heavy-ion reactions and give a reasonable account of experimental data obtained over a large incident energy and target-mass range.

In the present work, we aim to investigate about the contribution of direct processes, pre-equilibrium emission and evaporation of particles at such a high incident energy. One of the most widely used code package for simulations of nuclear reaction is TALYS. But it is still a work in progress and doesn't yet have the ability to completely describe heavy ion reactions. Also, the code works well for emission of protons and neutrons but when applied to ^{3}He, alpha particles or heavier ejectiles the results are disappointing [6–8]. Another very promising simulation code is ALICE [9–12] which is based on Monte Carlo simulations of the geometry-dependent hybrid (GDH) model for pre-equilibrium calculations and Weisskopf-Ewing model for the evaporation emission part. It works well at incident energies below 250 MeV, for light as well as heavy incident projectiles. It doesn't take into account the contribution from direct reactions but considers pre-equilibrium emission as well as thermal evaporation. We have investigated the pre-equilibrium reaction mechanism in the past by studying the excitation functions and neutron emission and have obtained satisfactory results using the version ALICE2014 [13,14]. But for our current work ALICE2014 under predicts the experimental data by a very large amount, suggesting that there are other possible dominant reaction mechanisms which contribute to the emission of alpha particles at energies presented in this paper.

Recently, a theoretical approach have been developed by O.V. Fotina, et al. [15] based on Griffin's model of non-equilibrium processes to describe the spectra of nucleons and other light particles emitted in the non-equilibrium stage of compound nucleus formation. They also took into account the contribution coming from the equilibrium stage of the process within the framework of the statistical model. For this purpose the statistical code PACE was modified [16] to accommodate the pre-equilibrium process calculations at sufficiently high energies. It is well known that PACE [17] implements the Hauser–Feshbach formalism to calculate the emission of light particles in the equilibrium stage. Furthermore, the probability of clustering of alpha particles [18–20] inside the projectile was also taken into account to describe the experimental double-differential spectra in a better way.

2. Theoretical model

In the Griffin's model of nuclear reactions, the relaxation of the compound nucleus to the equilibrium state is described by the master equation given by:

$$\frac{d}{dt}q\,(n,t) = \sum_{m=n-2}^{m=n+2} \lambda_{m\to n} q\,(m,t) - q(m,t)\left(w\,(n) + \sum_{m=n-2}^{m=n+2} \lambda_{n\to m}\right)$$

where $q\,(n,t)$ is the occupational probability for the composite nucleus state n, $w\,(n)$ is the emission rate of light particles, $\lambda_{m\to n}$ is the internal transition rate. $\lambda_{m\to n}$ are determined by the matrix elements of the transitions, $\langle |M|^2 \rangle$, and the density of exciton states to which the transition occurs which are in turn determined by single particle level density g. The single particle level density g is related to the level density parameter a in Fermi gas model by the relation $g = 6a/\pi^2$. Here we have regarded three values as free parameters, the transition matrix element, the single particle level density and the initial exciton configuration. In our case we used initial exciton number as $n_0 = 15\ (14p, 1h)$. The pre-equilibrium processes have been accommodated in the code for the estimation of double differential cross section. Furthermore, the probable effect of the clustering process of the projectile nucleus on the yield of secondary alpha particles have also been added. The emission of alpha particles at equilibrium was calculated using the Hauser-Feshbach formalism as included in the PACE code. A detailed theoretical description of the model can be found in O.V. Fotina, et al. [15].

3. Experimental procedure

The experiment was performed at the cyclotron facility of the iThemba LABS, Somerset West, South Africa, where the beam of ^{14}N ions of 250 MeV energy was supplied. A detailed description of the facility can be found in J.V. Pilcher, et al. [21]. The beams were focused on the target mounted at the centre of a 1.5 m diameter scattering chamber. The targets were mounted in aluminium frames with 25 mm diameter apertures. The ^{93}Nb and ^{59}Co target thicknesses were 1.72 mg/cm^2 and 1.00 mg/cm^2, respectively. A set of two $\Delta E - E$ Si surface-barrier detectors were used for particle identification, whose thicknesses were selected in such a way so as to cover both a lower and a higher energy region. One telescopes had thicknesses of 30 μm and 500 μm while the other had thicknesses of 100 μm and 2000 μm, respectively. Both detectors were mounted on two rotatable arms inside the scattering chamber on opposite sides of the beam and in the same reaction plane. By combining the data from both the telescopes, complete energy spectra was obtained. Other details of the detector arrangement and electronics used in the experiment can be found in the paper of another similar type of experiment performed here [5]. Data were acquired at various scattering angles ranging from 8°-120°. The overall systematic uncertainty of the absolute cross section values is estimated to be less than 10%.

4. Results and discussion

Figs. 1 and 2 show energy spectra of alpha particles at various angles in the reaction of ^{14}N with ^{59}Co and ^{93}Nb at an incident energy of 250 MeV. It can be seen that at very forward angles (8°-15°) the cross-section remains almost constant between 40 MeV to 80 MeV, while for alpha-particles emitted with energies above 80 MeV, there is a rapid decrease in the cross-section

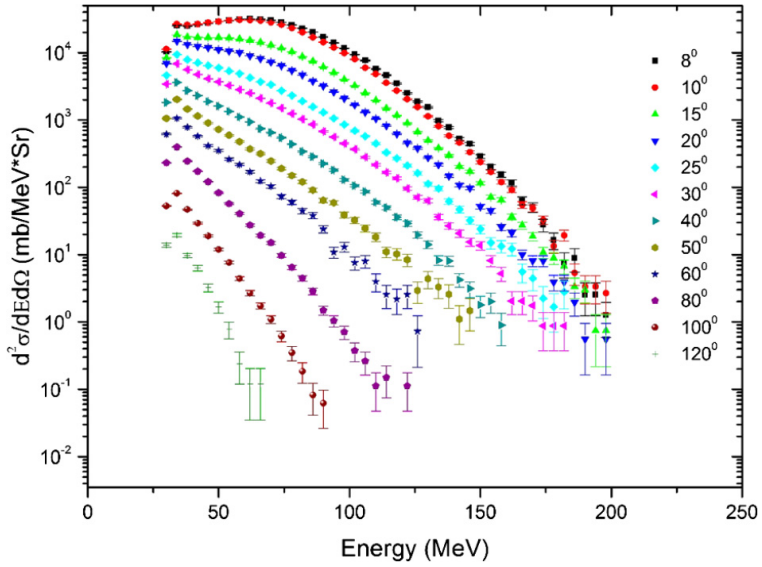

Fig. 1. Experimental double differential α-particle spectra for the interaction of ^{14}N with ^{59}Co at incident energy of 250 MeV.

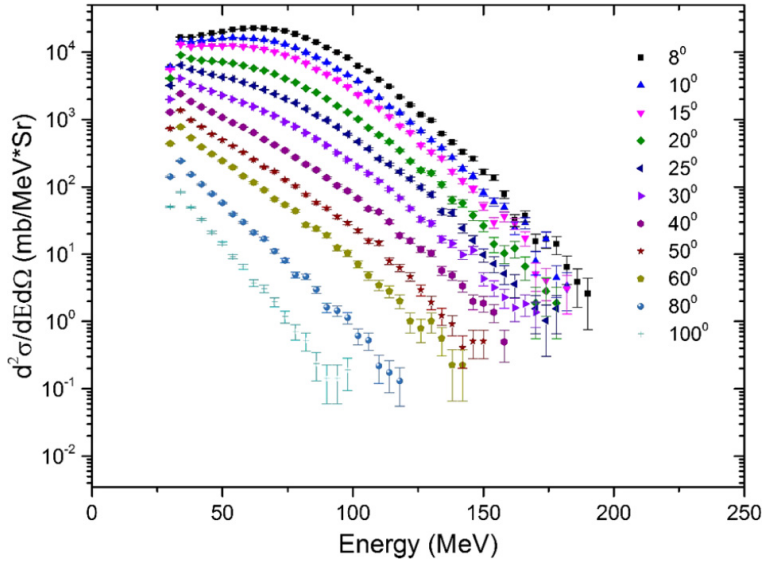

Fig. 2. Experimental double differential α-particle spectra for the interaction of ^{14}N with ^{93}Nb at 250 MeV.

as the energy increases. But at higher angles there is no such type of constant region and the cross-section keeps on decreasing rapidly with alpha particle energy right from the start. This trend is seen because of the spectator alpha particles, which are produced in the breakup of the projectile, and whose contribution decreases very rapidly at relatively larger angles (> 20°) as seen in the literature [22,23]. It is these spectator alphas which are responsible for high energy tail.

The "flat" region of the low energy alphas in the forward angle curves can be said to have majority of contribution from alphas which are re-emitted with reduced energy after undergoing incomplete fusion. These are created in the breakup of the projectile and, at incident energy used in present study and higher, there are high chances that they will not get dissociated immediately in the target nucleus after fusion and will survive for a few interactions with the nucleons and will get re-emitted with reduced energy in the forward cone. Results indicates that there is ∼50-70%

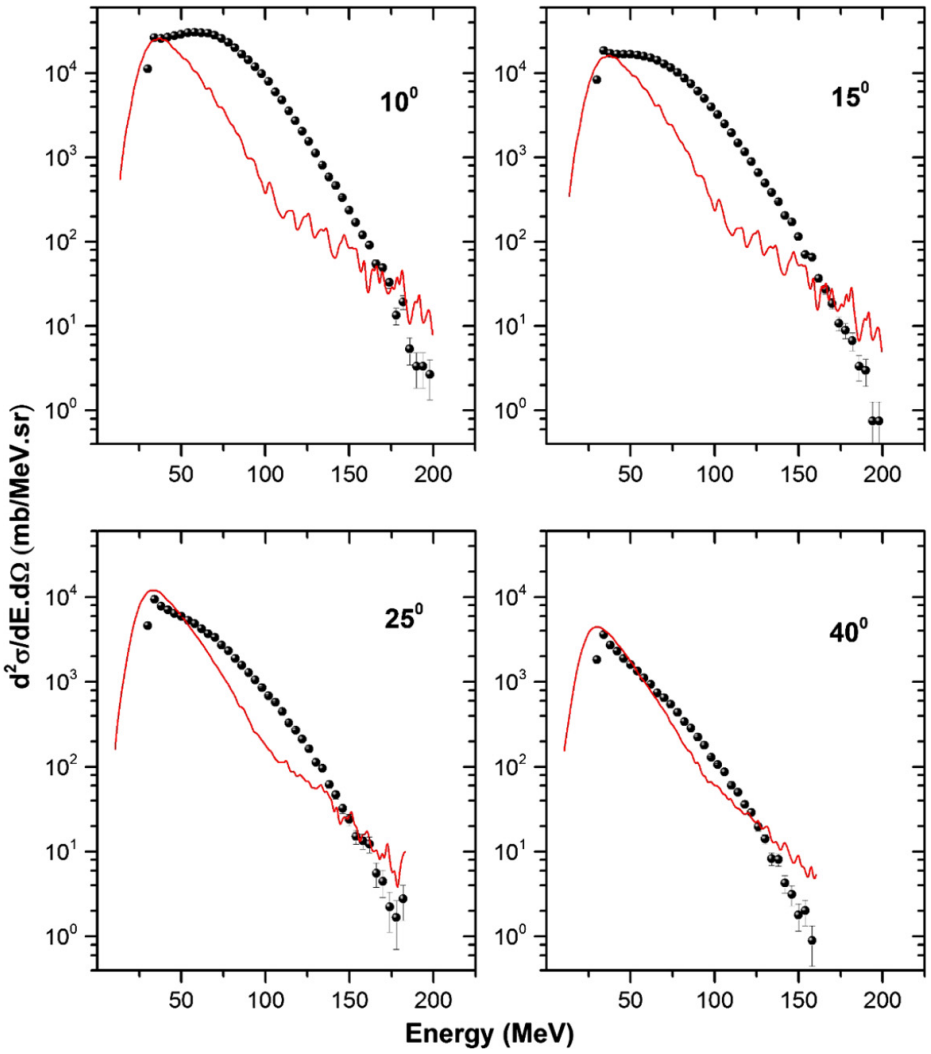

Fig. 3. Comparison between experimental and theoretical double differential α-particle energy spectra for the interaction of ^{14}N with ^{59}Co at an incident energy of 250 MeV at various angles. Solid spheres (black) are experimental data points which include error bars and the results of modified PACE4 are shown as solid curve (red). (For interpretation of the colors in the figure(s), the reader is referred to the web version of this article.)

decrease in energy of alpha particles after the fusion, when they are re-emitted. As we go towards higher angles, it is seen that the contribution of alpha particles coming from break-up decreases drastically and re-emission and pre-equilibrium emission becomes dominant mode of emission.

As shown in Figs. 3 and 4 we have compared our experimental results for ^{59}Co target with the modified PACE code which takes into account equilibrium and pre-equilibrium processes. At forward angles (15° and 25°) there is a large underestimation by the code as in this region the contribution from direct reactions are very much dominant. But as we go towards higher angles (above 40°) this underestimation reduces, as the contributions from direct reaction decreases and pre-equilibrium emission become the dominant modes of alpha particle emission within the range of 40° to 80°. At even larger angles (backward angles) the contribution of pre-equilibrium alpha particles also becomes negligible as mostly only emission from the equilibrium state persists.

Figs. 5 and 6 show the comparison of experimental data with predictions by the modified PACE code for the ^{93}Nb target at various angles. These spectra show a similar trend as that of

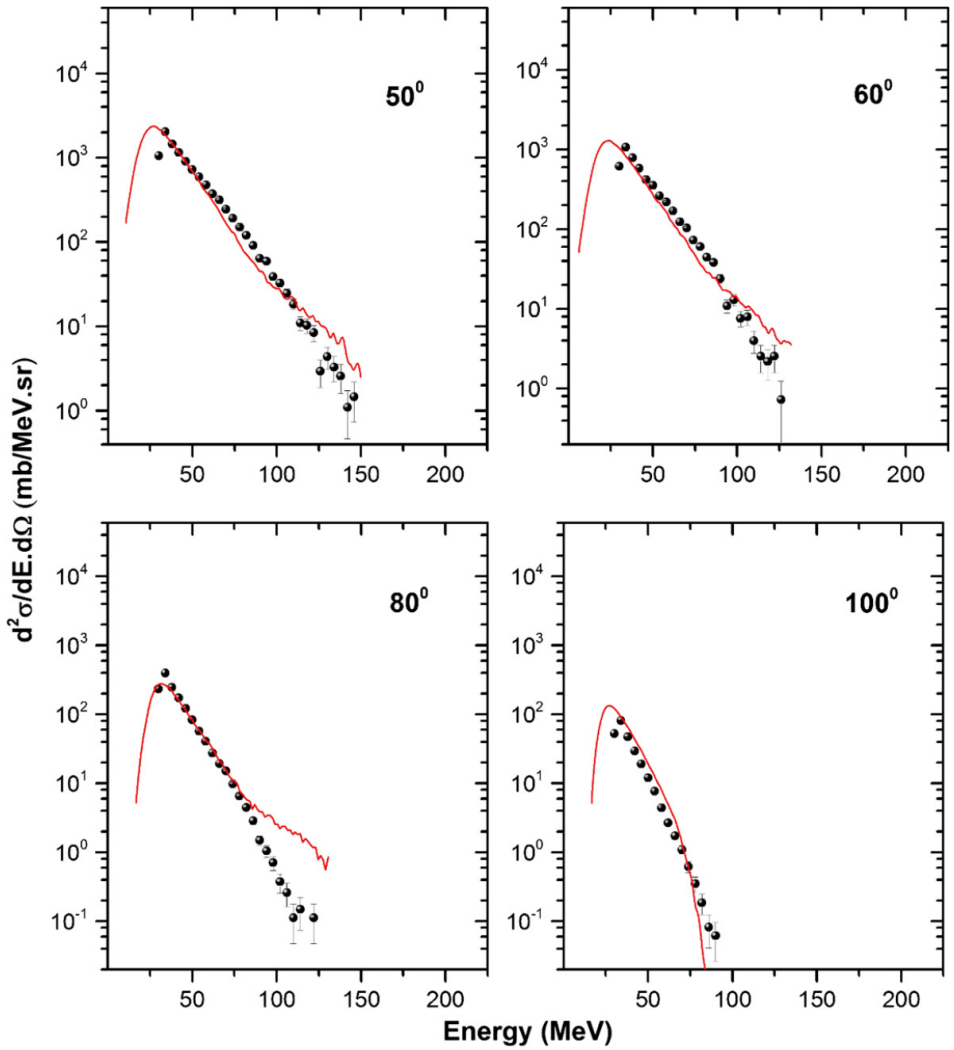

Fig. 4. Comparison between present experimental double differential α-particle energy spectra for the interaction of ^{14}N with ^{59}Co at 250 MeV (solid symbols) and modified PACE4 (solid lines).

^{59}Co. The dominant alpha emission mechanism in various regions is same as that in the case of ^{59}Co.

Fig. 7 shows the angular distribution of alpha particles for various emission energies. It can be seen that alpha particles with energies more than 150 MeV are not emitted at emission angle more than $\sim$50°. As the emission energy increases the angular distribution becomes more and more forward peaked. In the emission region below 150 MeV, re-emission after incomplete fusion, pre-equilibrium and evaporation emissions becomes dominant mode of emission. Majority ($\sim$90 %) of alpha particles emitted have relatively low energies (below 90 MeV) which means pre-equilibrium and evaporation mechanism are the major contributors to the emission of alpha particles as compared to direct processes.

5. Conclusions

In the present work, we have measured experimental double differential cross-sections for the secondary alpha particles emitted from the reactions ^{14}N + ^{59}Co and ^{14}N + ^{93}Nb at an incident beam energy of 250 MeV and compared them with theoretical predictions obtained using the modified PACE code, in order to probe alpha-particle emission in the pre-equilibrium

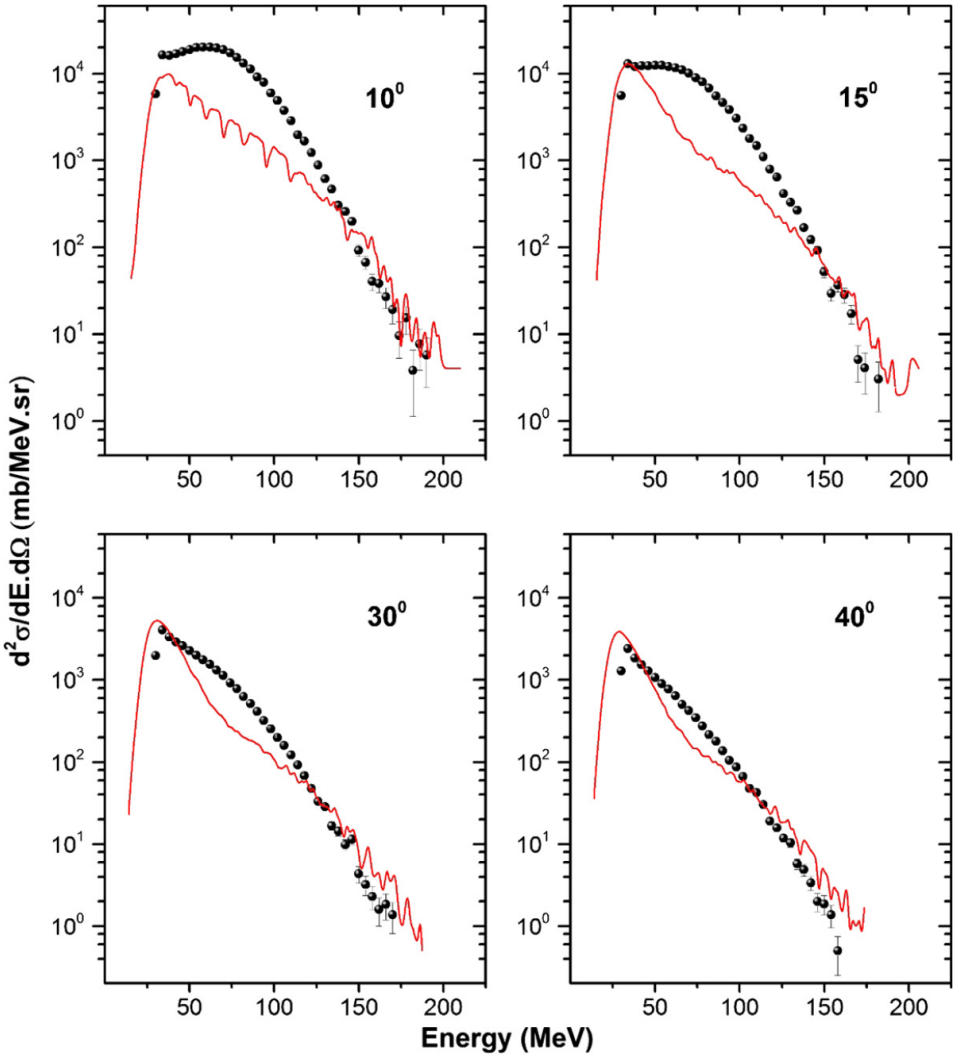

Fig. 5. Comparison between experimental and theoretical double differential α-particle energy spectra for the interaction of ^{14}N with ^{93}Nb at an incident energy of 250 MeV at various angles. Solid spheres (black) are experimental data points which include error bars and the results of modified PACE4 are shown as solid curve (red).

mode. From the study of the present results it can be inferred that at such a high incident energy, significant contribution to the alpha particle emission comes from direct reactions and re-emission of alpha after incomplete fusion and these mechanisms are dominant in forward angles. Towards larger emission angles the contributions from non-equilibrium and evaporation processes increase and start competing with direct reactions. There is a large amount of underestimation seen at forward angles and overestimation in some cases at backward angle. The modified PACE code used for comparison still needs inclusion of other reaction mechanisms to explain the experimental data in a better way, as it still under predicts the data by a large amount in certain regions. Hence further modifications are required on the code so that we can have a better nuclear model code that can predict the outcomes of heavy-ion induced reactions for the incident particle energies above 200 MeV. In fact, it is expected that the obtained experimental results are the basis for continuing research on the over production of alpha particles in heavy-ion induced reactions for the higher incident particle energies reactions.

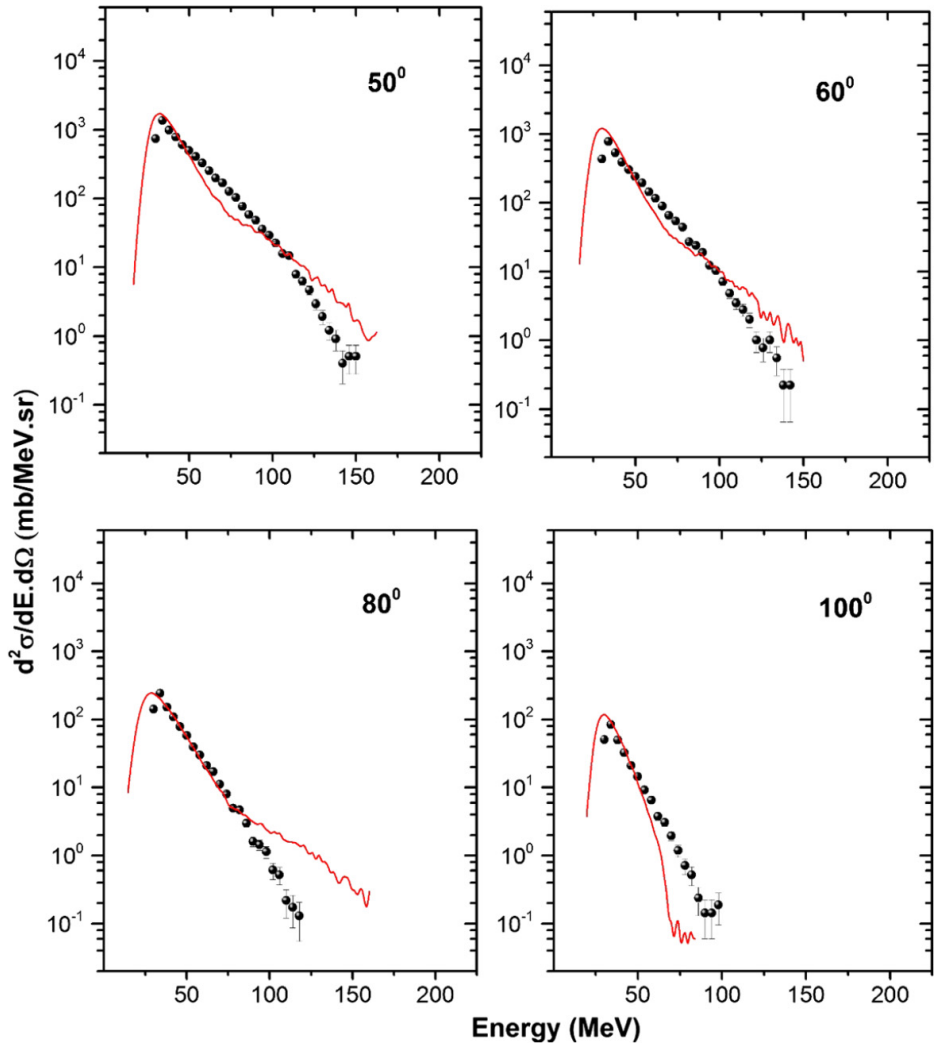

Fig. 6. Comparison between present experimental double differential α-particle energy spectra for the interaction of ^{14}N with ^{93}Nb at 250 MeV (solid symbols) and modified PACE4 (solid lines).

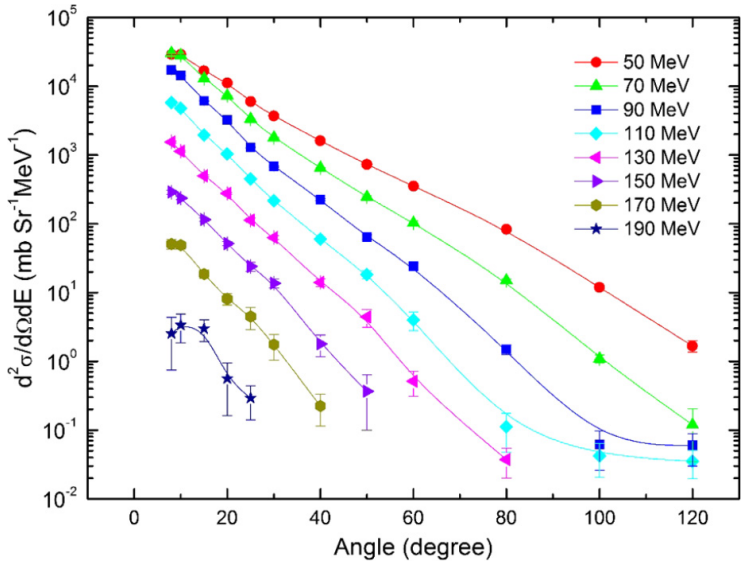

Fig. 7. Experimental angular distribution of α-particles emitted in the interaction of ^{14}N with ^{59}Co at 250 MeV.

Declaration of competing interest

We wish to confirm that there are no known conflicts of interest associated with this publication and there has been no significant financial support for this work that could have influenced its outcome.

References

[1] D.S. Ginger, K. Kwiatkowski, G. Wang, W.C. Hsi, S. Hudan, E. Cornell, R.T. de Souza, V.E. Viola, R.G. Korteling, Phys. Rev. C 78 (2008) 034601.
[2] H.C. Britt, A.R. Quinton, Phys. Rev. 124 (1961) 877.
[3] K. Siwek-Wilczynska, E.H. du Marchie van Voorthuysen, J. van Popta, R.H. Siemssen, J. Wilczynski, Nucl. Phys. A 330 (1979) 150.
[4] E. Gadioli, P.E. Hodgson, Pre-Equilibrium Nuclear Reactions, Oxford University Press, New York, 1992.
[5] E. Gadioli, M. Cavinato, E. Fabrici, E. Gadioli Erba, C. Birattari, I. Mica, S. Solia, G.F. Steyn, S.V. Förtsch, J.J. Lawrie, F.M. Nortier, T.G. Stevens, S.H. Connell, J.P.F. Sellschop, A.A. Cowley, Nucl. Phys. A 654 (1999) 523.
[6] R. Bevilacqua, PhD Thesis, Uppsala University, 2011.
[7] A.A. Cowley, G.J. Arendse, J.W. Koen, W.A. Richter, J.A. Stander, G.F. Steyn, P. Demetriou, P.E. Hodgson, Y. Watanabe, Phys. Rev. C 54 (1996) 778.
[8] A. Budzanowski, M. Fidelus, D. Filges, F. Goldenbaum, H. Hodde, L. Jarczyk, B. Kamys, M. Kistryn, St. Kistryn, St. Kliczewski, A. Kowalczyk, E. Kozik, P. Kulessa, H. Machner, A. Magiera, B. Piskor-Ignatowicz, K. Pysz, Z. Rudy, R. Siudak, M. Wojciechowski, Phys. Rev. C 80 (2009) 054604.
[9] M. Blann, Phys. Rev. C 54 (1996) 1341.
[10] M. Blann, M.B. Chadwick, Phys. Rev. C 57 (1998) 233.
[11] M. Blann, M.B. Chadwick, Phys. Rev. C 62 (2000) 034604.
[12] M. Blann, A.Y. Konobeev, Pre-compound cluster decay in HMSALICE, available in documentation supplied with RSICC code package PSR-550 (package name ALICE 2014/ALICE 2017), https://rsicc.ornl.gov/codes/psr/psr5/psr-550.html (unpublished).
[13] J. Acharya, S. Mukherjee, G.F. Steyn, N.L. Singh, A. Chatterjee, Phys. Rev. C 93 (2016) 024608.
[14] J. Acharya, S. Mukherjee, A. Chatterjee, N.L. Singh, Phys. Rev. C 97 (2018) 034607.
[15] O.V. Fotina, D.O. Eremenko, Yu.L. Parfenova, S.Yu. Platonov, O.A. Yuminov, V.L. Kravchuk, F. Gramegna, S. Barlini, G. Casini, M. Bruno, M. D'Agostino, O. Wieland, A. Bracco, F. Camera, Int. J. Mod. Phys. E 19 (2010) 1134.
[16] I.M. Egorova, S.O. Eremenko, S.Yu. Platonov, O.V. Fotina, O.A. Yuminov, Bull. Russ. Acad. Sci., Phys. 66 (2002) 1622.
[17] A. Gavron, Phys. Rev. C 21 (1980) 230.
[18] O.V. Fotina, S.A. Goncharov, D.O. Eremenko, S.Yu. Platonov, O.A. Yuminov, V.L. Kravchuk, F. Gramegna, T. Marchi, M. Cinausero, M. D'Agostino, M. Bruno, G. Baiocco, L. Morelli, M. Degerlier, G. Casini, S. Barlini, S. Valdrè, S. Piantelli, G. Pasquali, A. Bracco, F. Camera, O. Wieland, G. Benzoni, N. Blasi, A. Giaz, A. Corsi, D. Fabris, EPJ Web Conf. 66 (2014) 03028.
[19] D. Fabris, F. Gramegna, T. Marchi, M. Degerlier, O.V. Fotina, V.L. Kravchuk, M. D'Agostino, L. Morelli, S. Appannababu, G. Baiocco, S. Barlini, M. Bini, A. Brondi, M. Bruno, G. Casini, M. Cinausero, N. Gelli, R. Moro, A. Olmi, G. Pasquali, S. Piantelli, G. Poggi, S. Valdrè, E. Vardaci, Acta Phys. Pol. B 46 (2015) 447.
[20] D. Fabris, F. Gramegna, M. Cicerchia, T. Marchi, S. Barlini, S. Piantelli, M. Bini, M. Bruno, G. Casini, M. Cinausero, M. D'Agostino, M. Degerlier, N. Gelli, G. Mantovani, L. Morelli, J. Mabiala, A. Olmi, G. Pasquali, G. Poggi, S. Valdrè, E. Vardaci, O.V. Fotina, V.L. Kravchuk, M. Colonna, A. Ono, EPJ Web Conf. 163 (2017) 00016.
[21] J.V. Pilcher, A.A. Cowley, J.J. Lawrie, D.M. Whittal, Phys. Rev. C 40 (1989) 1937.
[22] G.D. Westfall, Z.M. Koenig, B.V. Jacak, L.H. Harwood, G.M. Crawley, C.K. Gelbke, B. Hasselquist, W.G. Lynch, A.D. Panagiotu, D.K. Scott, H. Stöcker, M.B. Tsang, Phys. Rev. C 29 (1984) 861.
[23] B. Borderie, M.F. Rivet, I. Forest, J. Galin, D. Guerreau, R. Bimbot, D. Gardes, B. Gatty, M. Lefort, H. Oeschler, S. Song, B. Tamain, X. Tarrago, Nucl. Phys. A 402 (1983) 57.